Cell Reports

Article

A vascular-associated fibroblastic cell controls pancreatic islet immunity

Graphical abstract

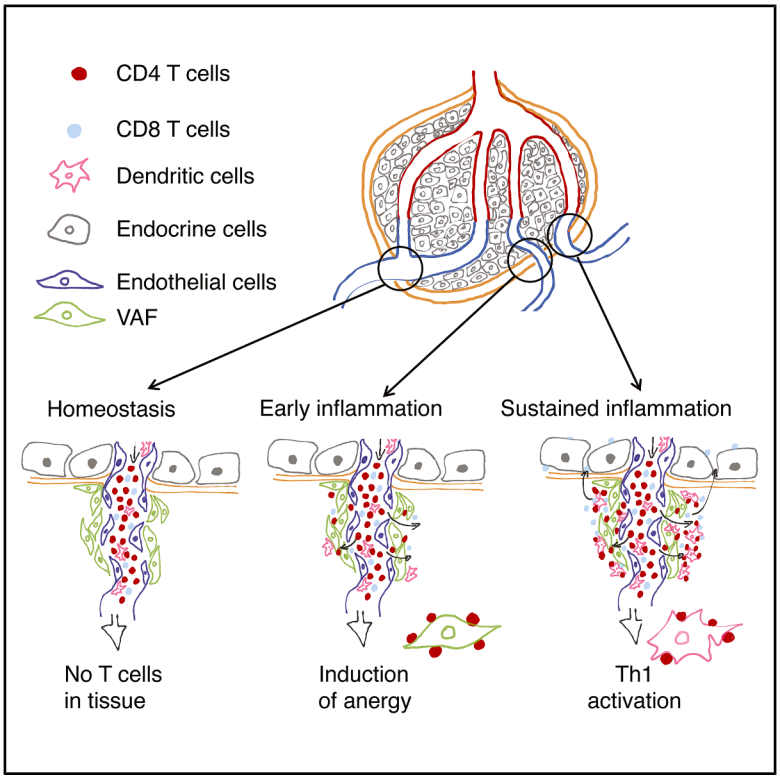

Authors

Don Clarke, Anne Costanzo, Siddhartha Sharma, ..., Christopher C. W. Hughes, Maike Sander, Luc Teyton

Correspondence

lteyton@scripps.edu

In brief

Clarke et al. reveal that non-hematopoietic cells, fibroblastic in nature, located outside the islet of Langerhans, spontaneously present β cell antigens. These cells, associated with the post-capillary venule, express PD-L1. Their potential role in immune modulation is shown by their induction of a tolerance program in pre-activated CD4 T cells.

Highlights

- Some CD45^{-} MHC class II-expressing cells, termed VAFs, are located outside of the islet
- VAFs are fibroblasts
- VAFs spontaneously present β cell peptide antigens
- VAFs express PD-L1 and can induce tolerance in CD4 T cells

Clarke et al., 2025, Cell Reports *44*, 116189
September 23, 2025
https://doi.org/10.1016/j.celrep.2025.116189

CellPress

Cell Reports

CellPress
OPEN ACCESS

Article

A vascular-associated fibroblastic cell controls pancreatic islet immunity

Don Clarke,[1] Anne Costanzo,[1] Siddhartha Sharma,[1] Lisa Kain,[1] Kelley W. Moremen,[2] Jeremy Pettus,[3] Alain Domissy,[4] Peng Wu,[5] Kim-Vy Nguyen-Ngoc,[6] Denise Berti,[6] Steven C. George,[7] Christopher C.W. Hughes,[8] Maike Sander,[6] and Luc Teyton[1,9,*]

[1]The Scripps Research Institute, Department of Immunology and Microbiology, La Jolla, CA 92037, USA
[2]University of Georgia, Department of Biochemistry and Molecular Biology, Athens, GA 30602, USA
[3]The Scripps Research Institute, DNA Array Core, La Jolla, CA 92037, USA
[4]University of California, San Diego, Medical School, San Diego, CA 92093, USA
[5]The Scripps Research Institute, Department of Molecular Medicine, La Jolla, CA 92037, USA
[6]University of California, San Diego, Department of Cellular and Molecular Medicine, La Jolla, CA 92037, USA
[7]University of California, Davis, Department of Biomedical Engineering, Davis, CA 95616, USA
[8]University of California, Irvine, Department of Molecular Biology and Biochemistry, Irvine, CA 92697, USA
[9]Lead contact
*Correspondence: lteyton@scripps.edu
https://doi.org/10.1016/j.celrep.2025.116189

SUMMARY

The immune protection of pancreatic β cells has three layers: anatomical, with their distribution in 1 million islets; central, with the thymic deletion of β cell-specific T cells; and peripheral, with inhibitory cellular networks. The failure of the latter leads to most spontaneous type 1 diabetes and all diabetes induced by checkpoint inhibitor therapy. Because CD4 T cells initiate disease, major histocompatibility complex (MHC) class II-expressing cells are central to the onset. In non-diabetic mouse and human islets, two such cells were detected outside of the islet boundaries near the efferent post-capillary venules: one related to the vasculature and a fibroblast referred to as a "vascular-associated fibroblast" (VAF). Functionally, primary VAFs spontaneously presented islet antigens to CD4 T cells and expressed high levels of inhibitory B7 receptors and no costimulatory receptors. VAFs induced anergy in primary pre-activated anti-islet CD4 T cells. VAFs are likely important to protect the endocrine pancreas from autoimmunity.

INTRODUCTION

The physiology of the pancreas was described in the first part of the 20th century and culminated with the discovery and characterization of insulin.[1] Fifty years later, the autoimmune nature of type 1 diabetes (T1D) was established based on pathology[2] and the discovery of anti-islet antibodies in polyendocrinopathies.[3] In 1987, the linkage between HLA class II genes and a single gene polymorphism at position β57 of the HLA-DQβ chain was revealed.[4] This association overwhelms all genome-wide association studies (GWASs)[5] and makes T1D the prototypical CD4 T cell-mediated autoimmune disease. Finally, most mechanistic studies pertaining to the pathology of T1D have been performed in the spontaneous rodent model, the non-obese diabetic (NOD) mouse, as it shares the most genetic risk factors with the human disease and, importantly, has aspartic acid loss at position β57 of its single major histocompatibility complex (MHC) class II molecule, I-A^{g7}.[4,6] Three facts, (1) ~1% of patients undergoing checkpoint-inhibitor-based immunotherapies for cancer treatment were concurrently developing clinical T1D,[7,8] (2) the same antibodies dramatically accelerate disease in NOD mice,[9] and (3) PD-L1-deficient humans develop T1D,[10] lead to the conclusion that tolerance to the islet, beyond incomplete thymic selection steps, is actively enforced in the periphery by negative regulatory loops, especially the PD-1/PD-L1 pair. Thus, it seems logical to posit that a PD-L1-positive (PD-$L1^{pos}$) cell expressing HLA class II is associated with the islet and protects it from immune attacks.

For decades, like most immunologists of T1D, our attention has been focused on the rare tissue-resident myeloid cells that are located within the double basement membrane (BM) that defines islets structurally.[11,12] These yolk sac-derived cells interact directly with α and β cells, have an activated phenotype, and participate in the phagocytosis of crinosomes to keep endocrine cells healthy.[11,13,14] Because myeloid cells express MHC class II, these resident macrophages/dendritic cells have the potential to present islet antigens to CD4 T cells *ex vivo*[12]; however, no evidence of *in vivo* CD4 T cell-macrophage interaction has ever been documented in tissue sections. In addition, we have recently shown that CD45-negative (CD45^{neg}) cells from the islets were capable of spontaneous presentation of islet antigens to CD4 T cells.[15] This observation made us reconsider the often-used term "T cell infiltration of the islet." Indeed, CD4 T cells are always or mostly located on the outside of the islet,[15–17] and

when CD8 T cells are seen in the confines of the islet, they are rare and isolated,[18] never associated with a typical inflammatory polymorphonuclear reaction as seen in most autoimmune lesions.[19] Moreover, following β cell destruction, the architecture of the islet is preserved, a feature that would be surprising after a destructive infiltrating process.

In order to explain these discrepancies, these observations were placed within the context of an often overlooked aspect of the pathophysiology of organs and tissues: that inflammation and extravasation of immune cells occur almost exclusively at the post-capillary venule side of the vasculature, where the endothelium is fenestrated.[20–22] In the case of islets, 5–6 collecting venules form and emerge from the islet proper and its outer BM.[23] Thus, it was hypothesized that this anatomical location would be where a regulatory PD-L1-HLA-II^{pos} cell would reside.

A combination of indirect immunofluorescence microscopy, single-cell isolation, and cell capture techniques was used to describe the islet-associated cells that spontaneously presented islet antigens. A new cell, called hereafter vascular-associated fibroblastic cells (VAFs), was discovered. Freshly isolated VAFs induced a tolerizing program in pre-activated CD4 T cells. This capacity was attributed to the absence of costimulatory receptors on VAFs and the delivery of an isolated signal 1 in the absence of signal 2 while signal 3 was present, a scenario known to lead to anergy.[24]

This series of experiments allows us to revise our views on the natural course of the elemental pathology of anti-islet immunity in T1D and propose a different model that may lead to new therapeutic approaches.

RESULTS

MHC class II expression in non-diabetic mouse and human islets

Unaffected NOD islets before the age of 10 weeks, as well as non-diabetic human islets from anonymous non-diabetic donors, were examined by indirect immunofluorescence and confocal microscopy for the presence of MHC class II^{pos} cells. The boundaries of islets and vascular components were located using the BM fibrillar component ER-TR7[25,26] (Figures 1A and 1B). In both species, most MHC class II^{pos} cells resided at the periphery of the islet and in the trabecular regions of large islets, where some efferent post-capillary blood vessels traverse (Figure 1B). These MHC class II^{pos} cells were intimately associated with the CD31^{+} vasculature (Figures S1A and S1B) and, more specifically, the draining venules identified by DARC/ACKR1 staining[27] (Figure S1C); in addition, some cells expressed inhibitory B7 family members such as CD274 (Figures 2A and 2B). B7-H3/CD276 and B7-H4 were also detected but were distant from the islet BM (Figures S2A and S2B). All B7 inhibitory family members were associated with the vasculature and the ER-TR7 BM. In mice, using staining of successive sections, the co-expression of PD-L1, ER-TR7, and MHC class II appeared likely (Figure S3).

Because they were tightly associated with the BM, the purification of those MHC class II^{pos} cells from non-diabetic mouse and human islets was difficult and poorly productive; after enzymatic digestion, a small number of cells could be stained, sorted by flow, and analyzed by SMART-seq RNA sequencing (RNA-seq)[28,29] (Figures 3A–3D). The cell sorting was performed after dissociation of the islets of 8-week-old mice and from 5 normal non-diabetic human donors. 192 CD45^{neg} MHC class II^{pos} single cells were isolated from NOD mice, with confirmed transcripts for 142 of them. In humans, 414 cells were recovered, and 288 were confirmed to express HLA-II transcripts. In each case, a small number of CD45^{pos} cells were used as a positive control (Figure 3). In mice, two CD45^{neg} populations emerged from the uniform manifold approximation and projection (UMAP): one related to endothelial cells and one marked by the expression of some epithelial/fibroblast genes (Figure 3A). The same two clusters were present in the human dataset along with 2 additional populations (clusters 0 and 1) that were assigned poorly to established lineages, did not express or poorly expressed measurable HLA class II transcripts, and were likely contaminants from the islet preparation (Figures 3B and S4). This mouse/human discrepancy could be partially explained by the techniques used to purify the islets. Mouse islets were hand-picked under the microscope to >95% purity and processed immediately, while human preparations, although fresh and shipped overnight, had purity values of 75%, 85%, 90%, 95%, and 95% for the 5 donors, respectively (purity was assessed by the provider). The RNA-seq experiments could not determine a convincing embryologic origin for the two main clusters of CD45^{neg}, MHC class II^{pos} cells.[30] Based on transcripts, the first one was identified as an epithelial fibroblastic cell (called VAFs), while the second one, endothelial in nature with expression of CD31, was called "vascular-related cell" (VRC). VAFs and VRCs shared the commonality of being CD45^{neg}, MHC class II^{pos}, PD-L1^{pos} (CD274) and/or B7-H3^{pos} (CD276) while expressing none of the classic CD80 and CD86 costimulatory molecules (Figures 3A–3D). It is important to note that in the mouse, RNA and protein sometimes disagreed for CD274 expression; indeed, transcripts were often below the level of detection, while protein could be detected. To confirm this observation, we sorted CD45^{neg}, MHC class II^{pos}, CD274$^{pos/neg}$ cells and repeated the SMART RNA-seq. These experiments across 6 mice confirmed that sometimes the PD-L1 protein was expressed without detectable transcripts or, more accurately, with transcripts that remain below detection levels (Figure S5).

What islet or islet-associated cells are spontaneously presenting islet antigens to primary CD4 T cells?

To interrogate the nature of the antigen-presenting cells (APCs) in islets, the recently developed FucoID technique, based on the fucosyl transferase (FucT)-mediated labeling of interacting cells, was used.[31] Anti-Ins$_{12\text{-}20}$ 8F10 or anti-BDC2.5 transgenic primary T cells were equipped with membrane-bound FucT (see STAR Methods), sorted by flow cytometry (Figure S6), and used to probe purified dissociated islets in a 2 h assay, without the addition of exogenous antigen. At the end of incubation, in the presence of the labeling substrate GDP-fucose-biotin, fucosylbiotinylated cells were sorted individually in 96-well plates (Figure 4A) and identified by qPCR using a 96-gene panel (see supplemental information) that qualified 5 populations: T cells, B cells, myeloid cells, VAFs, and VRCs (Figure 4B). MHC class II-blocking antibody was used in each experiment to evaluate

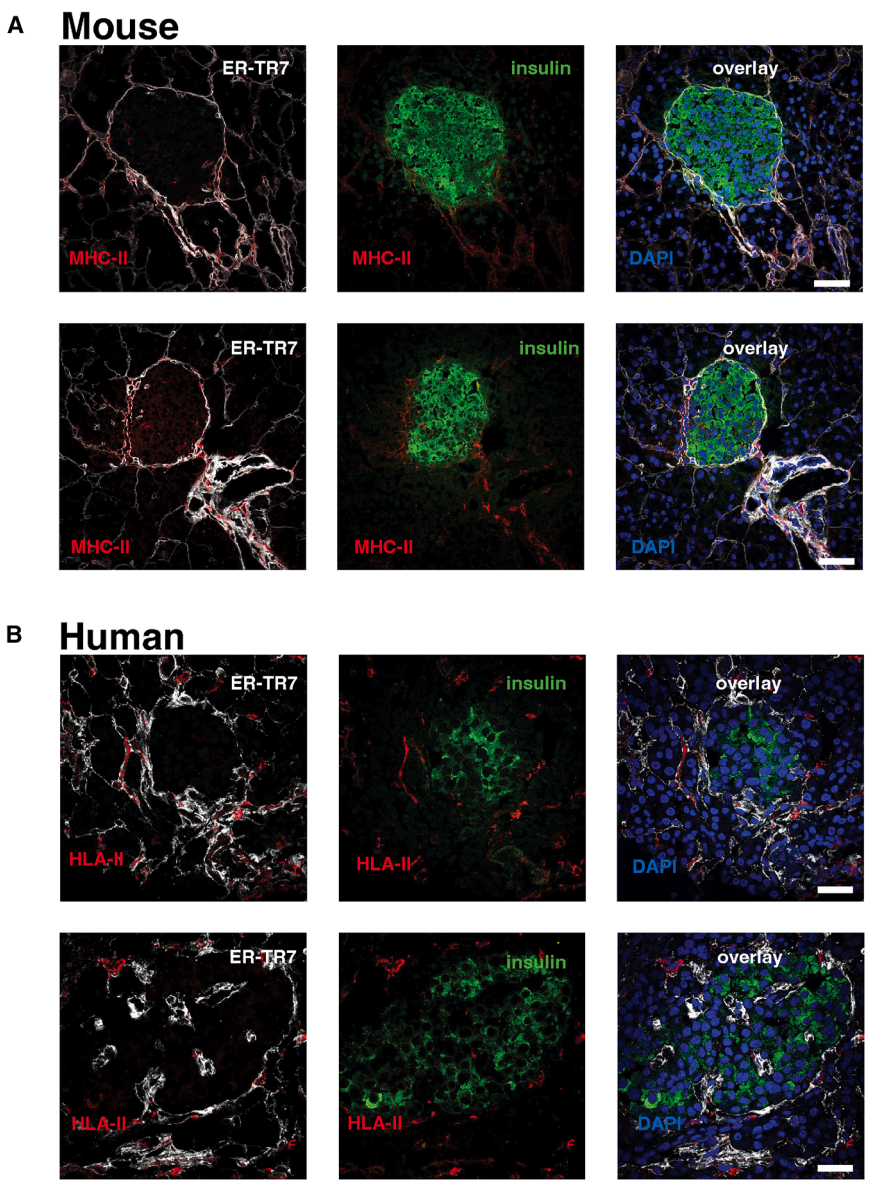

Figure 1. MHC class II-expressing cells are associated with the basement membrane that delineates the outside of mouse and human islets

(A) I-A^{g7}-expressing cells were detected in unaffected islets of 9-week-old NOD mice in association with the ER-$TR7^{pos}$ basement membranes of the islet and vasculature.

(B) Normal human islets showed a similar distribution of HLA class II-expressing cells associated with the ER-TR7 network.

Each fluorescent marker is indicated in each image. Scale bar: 50 μm.

the background (Figure 4A). Results obtained with 8F10 and BDC2.5 cells in 2 sets of independent experiments for each cell type were similar and are presented together. All labeling was performed on islets from 8-week-old NOD mice. While the starting cell pool was dominated by $CD45^{pos}$, MHC class II^{pos} cells over $CD45^{neg}$, MHC class II^{pos} cells (Figure 4C), 31.6% of the labeled cells were $CD45^{neg}$ and identified as VAFs based on their colocalization in the reference UMAP map (Figure S7). The remaining APCs were myeloid and B cells (48.7%), a very small percentage of VRCs cells (2.6%), and a few CD4 T cells (17.1%), which might be indicators of trogocytosis of MHC class II in the islet lesion[32] (Figure 4C).

Three conclusions were drawn: (1) although abundant, $CD45^{pos}$, MHC class II^{pos} myeloid cells were not the only APCs associated with the islet, (2) VRCs did not appear to have APC functions, confirming the literature,[33] and (3) VAFs, despite their low numbers and relatively low expression of MHC class II, appeared to be very productive APCs associated with the spontaneous presentation of two well-described islet antigens.

Stimulation of anti-islet CD4 T cells with intact islets

In view of these results, the classical "islet T cell stimulation assay" was revisited to try to compare the "outside versus inside" of islets for their capacity to engage T cells. Indeed, in its original form, this assay is always performed after dissociation of the islets, a step that is intended to free intra-islet myeloid cells from their environment and make them accessible to T cells for antigen presentation.[12] When non-dissociated islets were tested to stimulate anti-islet CD4 T cells, as few as 25 were sufficient to induce maximal IL-2 secretion of anti-islet CD4 T cell hybridoma (Figure S8). To extend this result with primary cells and provide more physiological answers, a new primary T cell assay based on single-cell transcriptomics was developed for naive and pre-activated T cells (Figure S9). Briefly, 3×10^4 anti-$Ins_{12\text{-}20}$ CD4 T cells from 8F10 transgenic animals were purified using negative selection and incubated without or with 150 whole islets from 8- to 9-week-old NOD, or NOD *H2-A*$^{-/-}$ (MHC class II knockout[34]), mice, in the presence of anti-I-A^{g7} antibodies (Figure 5). After a 5 h co-incubation, islets were excluded and CD4 T cells sorted as single cells by flow cytometry and examined by qPCR against a panel of 189 T cell activation genes.[35,36] At that time point, T cells associated and accumulated with islets in an MHC-dependent manner (Figures S10A and S10B). The merge of two independent experiments is shown in Figures 5A and 5B. Expectedly, naive 8F10 cells expressed CD4 T cell identity genes (CD3, CD4, CD27, CD28, CD40L, and CXCR4), some transcription factors important for T cell development (Foxo1, Runx1, and Lef1) but none for effector

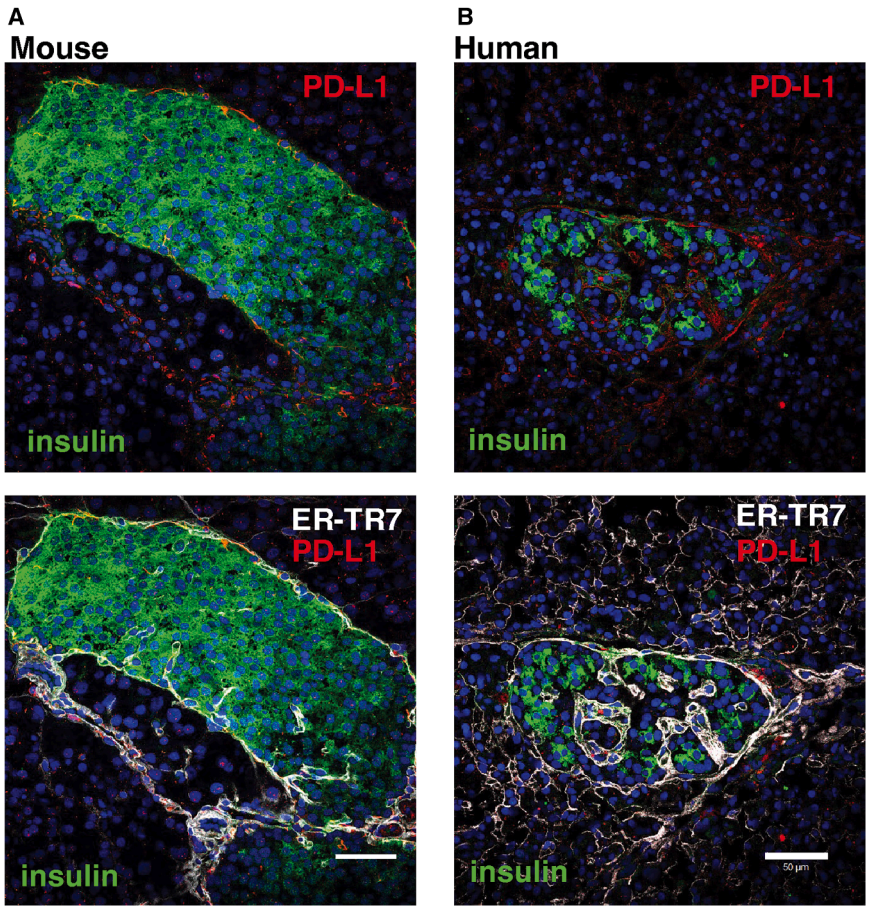

Figure 2. Expression of PD-L1 associated to the islet

Distribution of cells expressing the inhibitory member of the B7 family, PD-L1, in murine (A) and human (B) islets. For each section, the insulin stain is shown, as well as the ER-TR7 stain that highlights the basement membrane of the islet and vasculature. Scale bars: 50 μm.

function commitment, some basal signaling molecules (lck, lat, Fyn, Jak1, Plcg1, k-Ras, Akt1, Nfatc1, Mapk1, and Mapk3), many negative regulators of T cell activation (Ptprc, Pten, Ptpn6, Traf5, Tln1, Aim2, Gsk3a, and Gsk3b), and a set of tissue residency and self-renewal genes (Itga4, Il7r, Tcf7, Evl, Crip1, Arpc2, Sel1, S1pr1, and Klf2). Incubation with islets modified this transcriptional profile in two major ways. First, independent of T cell receptor (TCR) signaling and without significant induction of cell death relative to control (Figure S10C), the presence of islets next to 8F10 cells induced the silencing of the naive T cell signature (Figures 5A and 5B). Secondly, TCR recognition of $Ins_{12\text{-}20}$ presented spontaneously onto MHC class II molecules by islets driving the transcription of two families of genes, some linked to cytokine signaling (Stat3, Stat4, Stat5, and Socs3) and interferon response (Isg15, Oas1b, Oas2, Oasl1, Irf1, Ifit1, Ifit3, and Mx1) and some directly associated with TCR signaling (NfκB, Nur77, Zap70, Itk, Vav, Cd69, Cd25, Cccr4, Icos, Il-2, and Tnfα). Interestingly, only one function-committing transcription factor was upregulated: Bcl6. Tbx21- and interferon (IFN)γ-responsive genes remained silenced, and FoxP3 was expressed in only ∼10% of cells (see *p* values, Tables S3 and S4). Thus, this new format and deep interrogation of T cell activation with primary cells brought up two important results: the naive T cell transcriptome was heavily influenced by the presence of islets and naive cells were activated through their TCR without dissociation of the islets but also without induction of an overt Th1 phenotype.

The limitation of this assay was that it could not distinguish stimulation from either myeloid cells or VAFs. To address this issue, islets were dissociated and separated into $CD45^{neg}$ and $CD45^{pos}$ cells before being confronted with primary pre-activated 8F10 cells. For this purpose, purified 8F10 cells were activated in the presence of interleukin (IL)-2 through their TCR 8 days prior to being used in the primary islet cell assay. As seen in Figures 5C and 5D, the once-activated cells lost their signature of naivete (column 1) but displayed a full pattern of Th1 activation when in the presence of total dissociated islets from NOD mice (column 2); the disappearance of this signature with NOD *H2-A*$^{-/-}$ dissociated islets indicated the MHC class II dependence of this activation (column 3). When $CD45^{pos}$ cells were removed, the Th1 signature was nearly abolished and replaced by the expression of a unique set of genes (column 4) that were almost identical to the ones defining naive CD4 T cells (Figure 5A, column 1): Tcf7, Itga4, Lef1, Evl, Il7r, Cd28, Lat, Jak1, and S1pr1. This new pattern of activation was MHC class II restricted, as signified by its disappearance when 8F10 cells were stimulated by $CD45^{pos}$ depleted islet cells (column 5). Thus, this experiment revealed the presence of $CD45^{neg}$, MHC class II^{pos} cells in the islets capable of inducing tolerance.

The dominance of the hematopoietic antigen presentation and associated Th1 activation seen before CD45 depletion was likely explained by the much larger numbers of $CD45^{pos}$, MHC class II^{pos} cells associated with the islets at this particular time point (Figure 5E).

VAFs are phagocytic, present peptides but process antigen poorly

To get a better understanding of VAFs and the mechanisms controlling their MHC class II expression and function, a mouse cell line was produced by immortalizing sorted $CD45^{neg}$, $CD31^{neg}$, MHC class II^{pos} adherent murine islet cells with the large and small T antigens of SV40 in a scheme similar to the one used to establish fibroblastic reticular cell (FRC) lines.[37] The relatedness "cell line/primary cells" was established using the cell

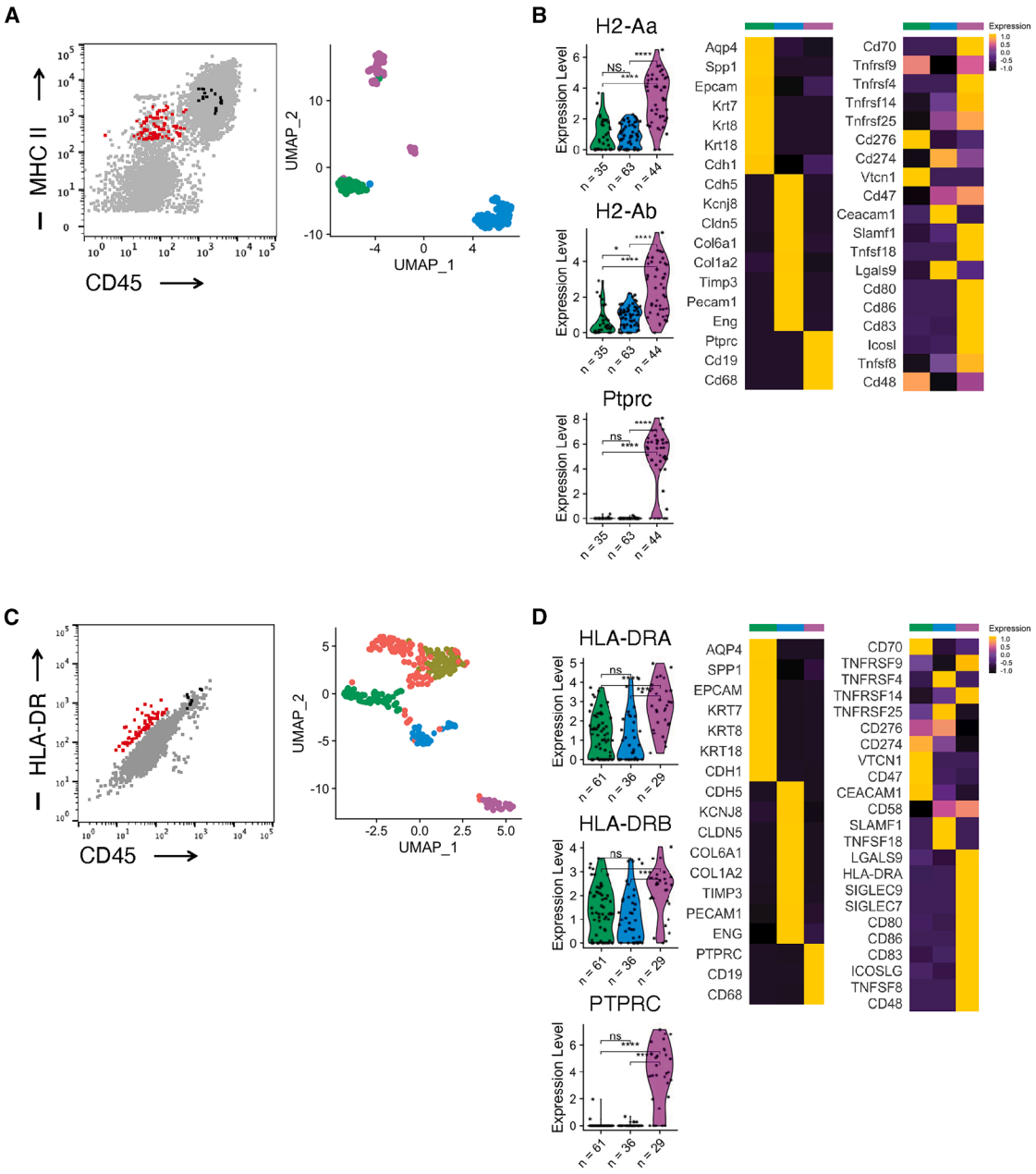

Figure 3. Expression of MHC class II by non-hematopoietic islet cells

Isolation and characterization of an islet-associated CD45^{-} MHC class II^{pos} cell in mouse (A and B) and human (C and D).

(A) In each experiment, CD45^{neg}/MHC class II^{pos} cells (red) were index sorted as single cells from pooled islets isolated from two 9-week-old NOD female mice. In each experiment, control CD45^{pos}/MHC class II^{pos} cells were also sorted and used for comparison. Accordingly, 3 populations were identified by unsupervised clustering as represented in the UMAP: fibroblastic cells (green cluster), vascular cells (blue cluster), and CD45^{pos} cells (purple cluster). Only cells that expressed MHC class II at the protein and transcriptional levels—98/114 CD45^{neg}/MHC class II^{pos} sorted cells and 44/50 CD45^{pos}/MHC class II^{pos} sorted cells—were analyzed. The UMAP retained 142 single cells.

(B) Violin plot representation of MHC class II α and β (H2-Aa and H2-Ab) and CD45 (Ptprc) expression in each of the 3 clusters. Each violin is the centered log ratio of normalized transcript.

(C) Left heatmap represents the most indicative genes for each of the 3 clusters. The right heatmap shows the expression of co-inhibitory and costimulatory T cell activation genes in each of the 3 clusters. Representative flow cytometry plot of CD45^{neg}/HLA-DR^{pos} cells index sorted (red) from normal non-diabetic human islets. CD45^{pos}/HLA-DR^{pos} cells were also sorted and used as controls. The UMAP representation shows all clusters for all cells isolated from 5 independent

(legend continued on next page)

identity panel described and validated in Figure 4 (supplemental information). As shown in Figure 6A, primary CD45^{neg}, MHC class II^{pos} cells could be split between "endothelial" and VAF subgroups by cytometry using CD31 and podoplanin as respective markers. Each of the CD45^{neg}, MHC class II^{pos}; double-negative; podoplanin^{pos}; and CD31^{pos} populations was sorted and profiled for gene expression. Then, the cell line was compared to primary skin fibroblasts at baseline and upon IFNγ stimulation by cytometry and gene expression (Figures 6A–6C). Then, all cell profiles were used to produce a UMAP and compare primary cells and the cell line, and five clusters were identified. First, this experiment showed the similarity between the cell line and the primary fibroblasts for their patterns of gene expression in IFNγ-non-treated and -treated cells. Second, and most importantly, the clustering showed a large share of genes (salmon cluster) between IFNγ-treated primary fibroblasts, IFNγ-treated cell line cells, and primary VAFs. This experiment validated the cell line and served to demonstrate the fibroblastic nature of the VAF cell and its plasticity. Indeed, MHC class II expression was not constitutive but only IFNγ inducible, and fibroblast identity genes such as Col1a1 and Col1a2 were repressed upon IFNγ stimulation in the cell line as well as in primary cells (Figure 6D). The phagocytic properties of the VAF cell line were demonstrated in a classic *in vitro* assay of pHrodo-labeled *E. coli* uptake (Figure 6E). Finally, the antigen presentation capabilities of the cell line were examined after I-A^{g7} induction with IFNγ and compared to splenocytes for both whole proteins and peptides. As seen in Figure 6F, while capable of presenting peptides, immortalized VAFs were not processing whole-protein antigen effectively.

Embryologic and lineage origins of VAFs

The plasticity of fibroblasts constitutes a huge hurdle to determining their embryonic lineage. Often associated with the mesoderm, fibroblasts can also differentiate from any epithelial tissue by a mechanism called "transition" and, thus, be produced from any of the three embryonic layers.[38] To address this issue for VAFs, we took advantage of our ability to differentiate *in vitro* pluripotent stem cells into endocrine pancreatic structures.[39,40] All protocols reach over 95% of endoderm commitment before the final steps drive endocrine differentiation.[41] In suspension, organoids were assembled in "pseudo-islet" structures in which α and β cells were found.[41]

At the basal state, no cells in the organoids expressed HLA-II molecules, while upon IFNγ stimulation, non-α, non-β cells did, and they localized mostly at the periphery of the pseudo-islets (Figure 7A). The HLA-II^{pos} cells were sorted and profiled by single-cell transcriptomics (Figures 7B and 7C). Their gene expression largely overlapped with primary VAFs from human islets, especially the cells from clusters 1 and 2, with correlation coefficients of 0.62 and 0.64, respectively (Figures 7D and S11).

DISCUSSION

In previous work, we made the surprising observation that from the islets of a single mouse, T cells expressing the same αβ TCR could differentiate to diametrically opposite sides of functional commitment, Th1 or regulatory T (Treg)[35]; this finding suggested strongly that the same antigen could be presented to CD4 T cells by two very different types of APCs, one activating and one inhibitory. To address this fundamental issue, single-cell technologies were applied to the characterization of the APCs associated with the islet, with the complement of confocal microscopy, the new FucoID technique,[31] and a single-cell-based transcriptomics assay to examine T cell activation. This latter approach was developed because the three assays commonly used to define the activation—upregulation of surface markers (CD25 and CD69), proliferation (^{3}H thymidine and CFSE dilution), and cytokine secretion (IL-2, ELIspot, and intracellular staining)—do not provide a good definition of tolerance, nor maintenance of tolerance. Therefore, it seemed appropriate to implement a single-cell, gene-signature-based assay that could define the various trajectories of CD4 T cells.

The first important information that we provide here is that MHC class II is expressed in normal murine and human islets by cells that are located at the periphery of the islet and associated with the efferent vasculature.[15] These cells are non-hematopoietic in origin based on their non-expression of CD45 and split into two families, vascular and fibroblastic, based on their gene transcription profiles, their morphology, and their location. The FucoID labeling experiment showed unambiguously that only VAFs were important in the spontaneous presentation of islet antigens, while the VRCs only played a minor role, if any, as published by others.[33] This discrepancy could be associated with the ability of the VAFs to capture secretory vesicles from the β cells thanks to their phagocytic capabilities, while endothelial cells, which are poor phagocytes, could not.[42] Interestingly, VAFs are poor antigen-processing cells but present peptides effectively. This observation reinforces the concept of Unanue that crinosomes are the main local source of autoantigens in the form of peptides and are central to the initiation of diabetes.[43–45] The second important element brought forward in the current study is the fact that MHC class II is not constitutively expressed by CD45^{neg} cells but is induced and lost in culture in a scenario reminiscent of FRCs.[37] The VAF cells share one additional similarity with FRCs: their association with both the activation and regulation/inhibition of CD4 and CD8 T cells.[46,47] Here, the induction of either phenotype is entirely dependent on the state of activation of the encountered T cell; naive CD4 T cells will receive some level of activation and may end up with a memory phenotype,[48] while memory antigen-experienced cells will be inhibited. It is evident from the series of experiments performed with pre-activated T cells (Figure 6) that when both CD45^{neg} and CD45^{pos}, MHC class II^{pos} cells

donors. Some exocrine pancreas contamination was present and produced 2 additional clusters (brown and red). 288/414 sorted cells expressed HLA-DR protein and transcript.

(D) Violin plot representation of MHC class II α and β (HLA-DRA and HLA-DRB1) and CD45 (PTPRC) expression for each of the 3 clusters. Violins are centered log-ratio-normalized counts. Left heatmap represents the most indicative genes for each of the 3 clusters. The right heatmap shows the expression of co-inhibitory and costimulatory T cell activation genes in each of the 3 clusters.

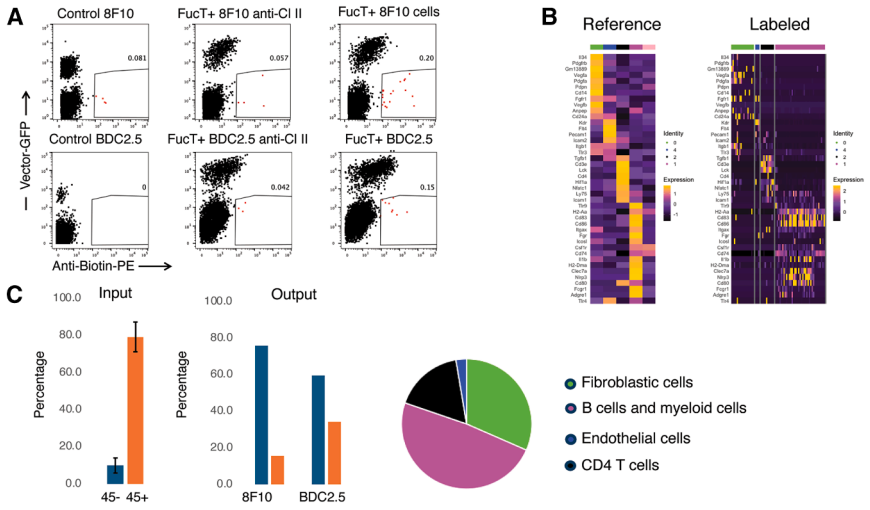

Figure 4. Labeling of primary antigen-presenting cells by primary anti-islet CD4 T cells equipped with membrane-bound fucosyl transferase

Following transduction with fucosyl transferase (FucT)-expressing or control empty vector, T cells were sorted by flow cytometry prior to being co-cultured with dissociated islets for 2 h.

(A) Representative flow cytometry plots of a labeling experiment at +2 h. Control was empty vector, FucT 8F10 cells were 8F10 CD4 T cells transduced with FucT, and anti-class II was anti-I-A^{g7} monoclonal antibody. An identical experimental setup was used for BDC2.5 CD4 T cells.

(B) Validation of a panel of 96 genes picked to identify potential antigen-presenting cells: VAF cells (green), endothelial cells (blue), myeloid cells and B cells (pink), and T cells (black). Validation was performed in two independent experiments using 159 $CD45^{neg}$/MHC class II^{pos}/$CD31^{neg}$/$PDPN^{pos/neg}$ fibroblastic cells, 45 $CD45^{neg}$/MHC class II^{pos}/$CD31^{pos}$/$PDPN^{neg}$ endothelial cells, 35 $CD45^{pos}$/$CD11b^{pos}$/MHC class II^{pos} myeloid cells, and 35 $CD45^{pos}$/$CD19^{pos}$/MHC class II^{pos} B cells.

(C) $CD45^{pos}$/$CD45^{neg}$ratio in input and output of the FucT labeling experiments. Input: MHC class II^{pos}/$CD45^{neg}$ (blue) and MHC class II^{pos}/$CD45^{pos}$ (orange) from the islets of 5 mice of similar age as those used for the labeling (7–9 weeks). The ratio $CD45^{+}$ versus $CD45^{-}$ is about 5:1. Output: MHC class II^{pos}/$CD45^{neg}$ (blue) and MHC class II^{pos}/$CD45^{pos}$ (orange) percentage after FucT labeling using either 8F10 or BDC2.5 T cells (2 independent experiments for each). In 8F10 mice, sorted $CD45^{pos}$ and $CD45^{neg}$ cells were in almost equal numbers, whereas in BDC2.5 mice, $CD45^{pos}$ cells were twice as many as $CD45^{neg}$ cells; these differences are likely due to different stages of disease progression in all the mice. As shown for both 8F10 and BDC2.5, MHC class II antibody blocking resulted in background staining (0.06% for 8F10 and 0.04% for BDC2.5). In total, 71 cells were usable for analysis out of 92 after 8F10 labeling and 67 out of 126 labeled after BDC2.5 labeling. The pie chart shows the distribution of cell types among the three APC categories, VAFs, myeloid, and B cells, for all cells from all experiments.

were present together in the assay, professional $CD45^{pos}$ cells were dominant and drove full Th1 activation, overwhelming the negative regulation of $CD45^{neg}$ cells (see synopsis in Figure S12). This result and the fact that, over the course of the disease, $CD45^{pos}$, MHC class II^{pos} cells were increasingly numerous favor a scenario in which the front of the pathology is dominated by negative regulation in an attempt to maintain tolerance. The influx of $CD45^{pos}$ cells in the vicinity of the islet when insulitis is built would overcome this negative regulation and promote the Th1 CD4 T cell phenotype. This activation/inhibition balance would govern islet destruction timing, as well as the course of disease, by allowing remissions and relapses (Figure S12). Mechanistically, VAFs appear to induce or maintain tolerance by expressing MHC class II and negative regulators, such as PD-L1, without expressing activating coreceptors. Once again, PD-L1 is shown to be critical for active islet tolerance as it has been in mouse models[9,49] and humans, genetically[10] or after CPI therapy.[7]

The hypothesis that T cell tolerance is dependent on the existence of three signals and their order of delivery has been proposed[50] and documented for decades[51–55] but has never been put in the context of control of organ protection and T1D. This view of the immune physiology of the islet and the active induction of tolerance is reinforced by the finding that in non-diabetic, at-risk HLA donors, the dominant circulating anti-insulin CD4 T cell population exhibits stigmas of partial T cell activation among a vast number of silenced genes.[48]

Because anti-islet autoimmunity is the exception, not the rule, it appears sensible to have a negative cellular regulator of T cell activation associated with a segment of the vasculature, the post-capillary collecting venule, where inflammation is sensed.[20,56] Such a protective system meant to enforce tolerance could be overwhelmed by the intensity/duration of inflammation, the affinity of some T cells,[57] the influx of professional APCs upon the formation of a tertiary lymphoid structure,[15] the modulation of coreceptor expression, or the pharmacological blockade of some key negative regulators.[7,9] It is also important to mention that the efficiency of this mode of protection of the islet is complemented by the absence of direct lymphatic drainage of the islet[15] and the physical separation of the islets throughout the pancreas, which limits immune cell access. The location of an APC directly outside of the islet and in close proximity to the exocrine pancreas could also explain some of the links that have been reported between exocrine and endocrine pancreas inflammation.[58,59]

When tolerance is broken, it is likely that islets are destroyed one at a time and that, in most scenarios, diabetes, in its clinical form, does not ensue. Without pretending that we uncovered the reason why the endocrine pancreas is split into ~1 million units, it makes sense to consider the protection of islets from injuries and autoimmunity as a multilayer system: isolation (no lymphatics and reliance on tertiary lymphoid structures, not the draining lymph node[15,35]), multitude with independence (each of the 1 million islets is autonomous), negative regulation of T cell activation by VAFs, and limited spreading of anti-islet responses by relying on tertiary lymphoid structures instead of a classical lymphatic drainage and lymph nodes that would amplify responses more readily. The co-development of the VAFs with the islets, as we observed in the human embryonic stem cell (hESC)-derived pseudo-islets, suggests the importance of those cells in evolution for the preservation of islet functions. The efficiency and

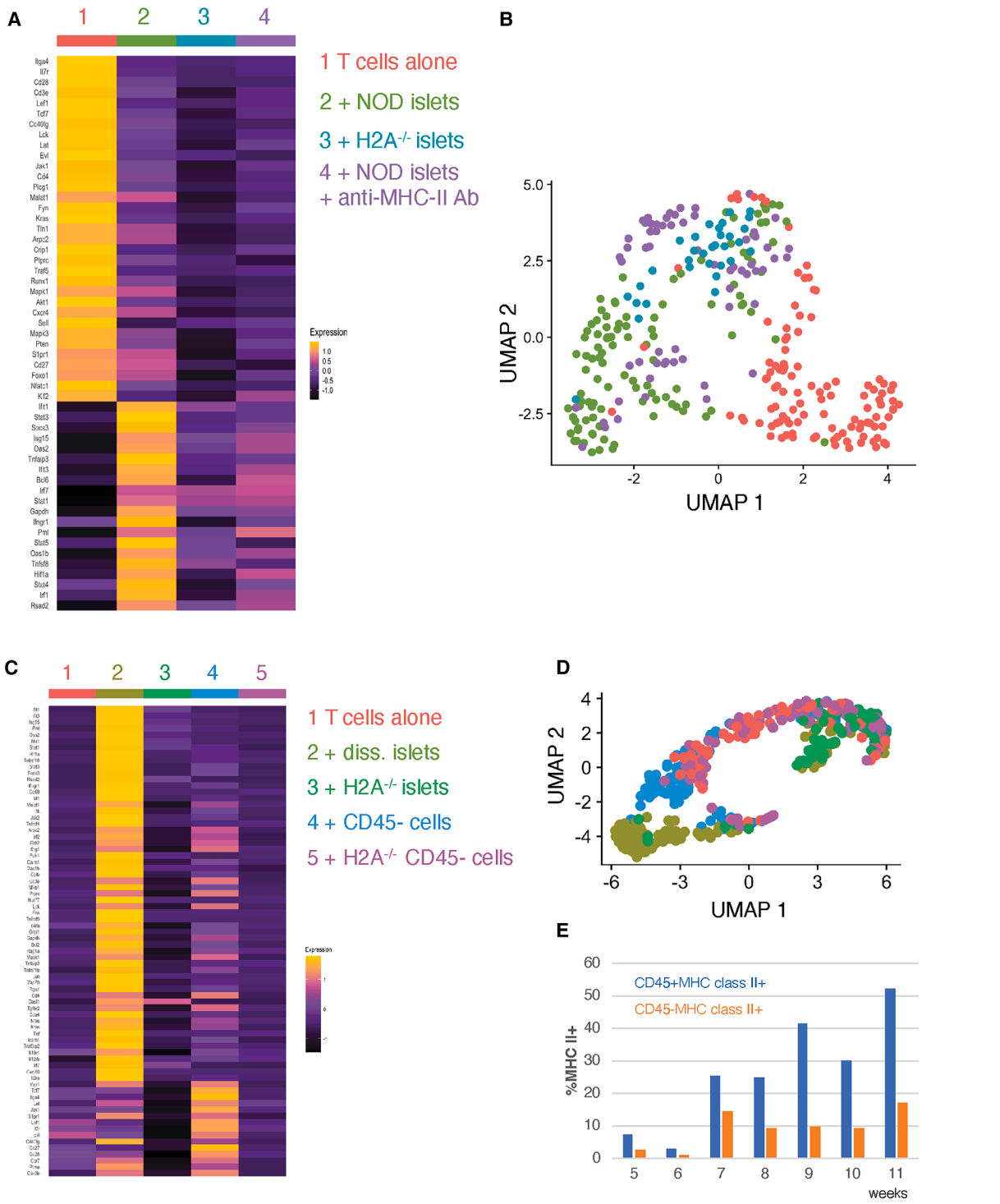

Figure 5. Single T cell analysis of the spontaneous antigen presentation by MHC-II^{pos} islets of Langerhans cells

(A) Activation of naive anti-insulin CD4 T cells by islet-associated cells. Heatmap shows averages from two independent experiments where 150 islets from 2 NOD female mice were pooled and co-cultured with CD4^{+} cells purified using negative selection from spleens of 8- to 10-week-old 8F10-NOD female mice. 98.7% (316/320) of the Vβ8.1/8.2^{pos}/CD4^{pos} single cells sorted from 4 experimental conditions were usable for analysis, of which 109 were 8F10 T cells alone, 112 were 8F10 cells with whole islets, 63 were 8F10 cell with whole islets and MHC class II-blocking antibodies, and 32 were 8F10 cells with whole islets from *H2-A*$^{-/-}$ mice. RT-qPCR was used to measure 189 genes per cell. The heatmap shows all differentially expressed genes ordered by *p* value, calculated using a Wilcoxon rank sum (Table S2).

(legend continued on next page)

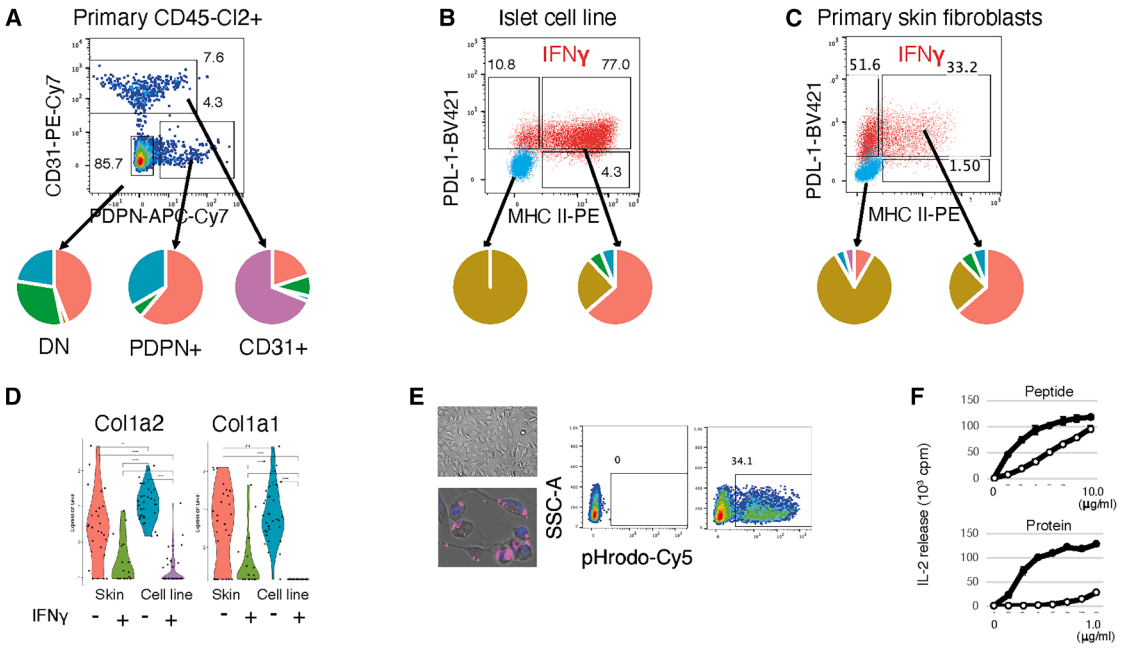

Figure 6. Pancreatic fibroblastic cell line characterization

(A) Representative flow cytometry plot of primary CD45^{neg}/MHC class II^{pos} cells from mouse islets, divided according to their CD31 and podoplanin expression; it separates three populations: double negative, endothelial (CD31), and VAF (podoplanin^{+}).

(B and C) Flow cytometry plots of the fibroblastic cell line (B) and primary skin fibroblasts (C) after IFNγ treatment. It shows the coordinated upregulation of MHC class II and PD-L1 on both cell types.

Each population in (A)–(C) was profiled by single-cell RT-qPCR against the 96 identity genes described in Figure 4 and clustered by *k*-means and nearest neighbor to produce a UMAP. Pie charts represent the distribution of each cell population in the 5 clusters defined by that profiling and colored. Upon IFNγ stimulation, both cell line and primary fibroblasts acquired profiles similar to the primary VAF cell shown in (A), with a large percentage of cells falling into the salmon cluster.

(D) Similar downregulation of Col1a1 and Col1a2 transcripts in the fibroblastic cell line and skin fibroblasts.

(E) The morphology of the fibroblastic cell line is shown in a bright-field image (top) and after phagocytosis of *E. coli* conjugated to pHrodo-Deep Red (bottom). The cytometry profile of that experiment is shown to the right.

(F) VAF cell line was compared to NOD splenocytes for the presentation of whole HEL protein or HEL_{11-27} peptide to the anti-HEL CD4 T cell clone 21.30. This assay was repeated twice with similar results. IL-2 was measured in supernatants at 24 h; each dilution of antigen was in triplicate.

resilience of this system probably explain why the pre-clinical phase of T1D is often so long.[60,61]

On the etiologic and therapeutic fronts, the present findings refocus attention on two associated features, inflammation and vasculature, of the pancreas. As an organ that is integral to the digestive system, the pancreas is exposed to permanent injuries from the food, microbes, environmental molecules, and drugs that we ingest.[15] For instance, increasing intestinal permeability experimentally is sufficient to increase the incidence and time of onset of T1D in mice.[15,62] Epidemiologically speaking, as the Western lifestyle increases potential pancreatic insults, a steady rise of T1D incidence has been observed,[63] together with an increase in pancreatitis[64] and pancreatic cancer,[65] two conditions also linked to local inflammation. Testing the impact of dietary and/or lifestyle changes on T1D incidence is nearly inconceivable or at least very difficult. However, it is becoming clearer that obesity is a contributing factor to T1D onset,[66] and removing pro-inflammatory short-chain fatty acids from the diet of at-risk individuals might be a beneficial first step. Conversely, it would also seem reasonable to increase the intake of anti-inflammatory food and/or drugs.[67] More invasive approaches, such as antibody treatment targeted at adhesion molecules of the vasculature, could also be considered, but their timing in pre-clinical populations would be a challenge.

(B) The UMAP of the 316 cells is shown with each cell color coded for each of the four conditions.

(C) VAF induction of anergy in activated anti-insulin CD4 T cells. Pre-activated 8F10 T cells were co-cultured with dissociated islets for 5 h in various conditions and sorted individually for RT-qPCR. 384 cells sorted from 5 conditions in 2 independent experiments were used for analysis: pre-activated 8F10 cells alone (64 cells), pre-activated 8F10 cells with dissociated islets (96 cells), pre-activated 8F10 cells with dissociated islets from *H2-A*$^{-/-}$ mice (64 cells), pre-activated 8F10 cells with islets depleted of CD45^{+} cells (96 cells), and pre-activated 8F10 cells with islets depleted of CD45^{pos} cells from *H2-A*$^{-/-}$ mice (64 cells). The heatmap shows all differentially expressed genes ordered by *p* value, calculated using a Wilcoxon rank sum.

(D) UMAP representation of the 384 cells color coded by experimental condition.

(E) Bar plot representation of the percentage of MHC class II^{pos}/CD45^{neg} or MHC class II^{pos}/CD45^{pos} cells isolated from the islets of NOD mice spanning 5–11 weeks. Each time point represents pooled islets from two mice.

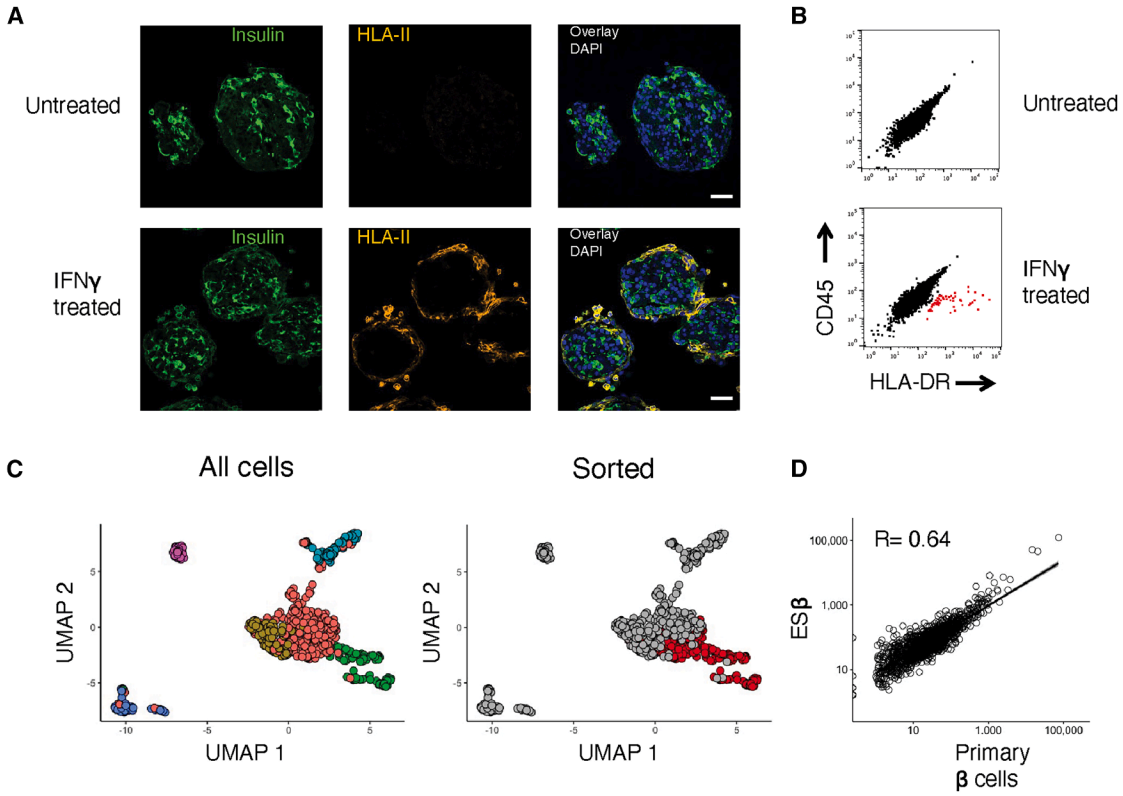

Figure 7. Differentiation of VAF-like cell from embryonic stem cells

(A) Differentiated H1 hESC pseudo-islets were treated for 72 h with or without 10 ng/mL IFNγ and flash frozen in OCT mounting media. 10 μm slices were stained for insulin (green) and HLA-DR (ochre) using DAPI for nuclear stain and imaged by confocal microscopy. Non-insulin secreting cells located at the periphery of the pseudo-islets expressed HLA-DR. Scale bar: 50 μm.

(B) HLA-DR-expressing cells were visualized by flow cytometry (red label) and single-cell sorted in 96-well plates after Accutase dissociation.

(C) RNA-seq of primary and hESC HLA-DR^{pos} cells were analyzed by unsupervised clustering, and 6 clusters were identified. On the right, hESC-derived cells are shown in red in an overlay representation.

(D) HLA-DR^{pos} hESC-derived cell RNA sequences showed a 0.64 correlation coefficient with cluster 2 of the normal HLA-DR^{+} population of non-diabetic islets.

Limitations of the study

Rare cell populations are always difficult to study. An added layer of difficulty in the current study is the association of VAFs with the post-capillary venules and the BM of the islet. Venules are fragile and can be lost during islet isolation, while enzymatic dissociation from the BM is often difficult. These factors are major impediments to an accurate enumeration of the cells. Our study shows the potential role of VAFs in tolerance induction in *in vitro* studies. This function will need to be demonstrated *in vivo* in further studies by knocking out MHC class II and/or PD-L1 in VAFs.

RESOURCE AVAILABILITY

Lead contact

Requests for further information and resources should be directed to and will be fulfilled by the lead contact, Luc Teyton (lteyton@scripps.edu).

Materials availability

All unique reagents generated in this study are available from the lead contact with a completed materials transfer agreement.

Data and code availability

- Single-cell RNA-seq and gene expression data have been deposited at Gene Expression Omnibus website (accession number GEO: GSE292898).
- No in-house code was used for this study.
- Any additional information required to reanalyze the data reported in this paper is available from the lead contact upon request.

ACKNOWLEDGMENTS

Thank you to Kenna Nagy and Lisa Kain for critical evaluation of the manuscript and insightful suggestions. We are very appreciative of Brian Monteverde and Brian Seegers of the Flow Cytometry Core at Scripps Research for spending late evenings running our samples. We are also grateful to the team of the DNA Array Core facility for providing technical support with the next-generation sequencing experiments. The authors are forever grateful to Emil Unanue for his critical discussions and intellectual input. Some tissues were provided by the Network for Pancreatic Organ Donors with Diabetes (nPOD; RRID: SCR_014641); nPOD is a collaborative T1D research project supported by JDRF (nPOD: 5-SRA-2018-557-Q-R) and the Leona M. and Harry B. Helmsley Charitable Trust (grants 2018PG-T1D053 and G-2108-04793). This work was supported by grants from the NIH: the Clinical and Translational Science Award issued to the Scripps Translational Science Institute; UL1TR002550 and TL1TR002551 to D.C. and S.S.; 1R01 GM130915 to K.W.M.; 1R01AI143884 to P.W.; 1R01DK117138 to L.T.; UH3 DK122639 to M.S., C.

C.W.H., and S.C.G.; BioF:GREAT, NSF 2400220 to K.W.M.; and UG3DK1421188 to C.C.W.H. and L.T.

AUTHOR CONTRIBUTIONS

Most experimental data were produced by D.C., including data analysis and graphics. D.C. also contributed to the writing of the paper. A.C. handled mouse islet cell preparations and all confocal imaging of tissues. L.K. maintained the NOD mouse colony and produced the MHC tetramers. K.W.M. produced the vectors used for the FucT assay. J.P. coordinated and was instrumental in the procurement of human tissues. A.D. performed computational analysis. P.W. provided guidance for the FucT assay. K.-V.N.-N., D.B., S.C.G., C.C.W.H., and M.S. contributed to the iPSC and ES work. S.C.G., C.C.W.H., and M.S. critically read/edited the manuscript, and L.T. wrote the manuscript. L.T. conceived the project and performed single-cell gene expression analysis. S.S. contributed to the single cell analysis and gene expression.

DECLARATION OF INTERESTS

The authors declare no conflicts of interest.

STAR★METHODS

Detailed methods are provided in the online version of this paper and include the following:

- KEY RESOURCES TABLE
- EXPERIMENTAL MODEL AND STUDY PARTICIPANT DETAILS
  - Mice
  - Cell lines
  - Human tissues
- METHOD DETAILS
  - Re-expression of TCRs in 5KC cells
  - T cell hybridoma stimulation assay
  - Primary T cell stimulation assays
  - Single-cell flow cytometry sorting for T cell assays
  - Fucosylation-biotinylation (FucoID) assay
  - Human islet single-cell flow cytometry and sorting
  - Mouse islet isolation and single-cell flow cytometry
  - SMART-seq2 library preparation
  - Primary skin fibroblast isolation
  - Immunofluorescence of frozen pancreatic sections
  - Phagocytosis assays
  - Maintenance and differentiation of H1 hESCs (procedure)
- QUANTIFICATION AND STATISTICAL ANALYSIS

SUPPLEMENTAL INFORMATION

Supplemental information can be found online at https://doi.org/10.1016/j.celrep.2025.116189.

Received: September 23, 2024
Revised: June 30, 2025
Accepted: August 1, 2025

REFERENCES

1. Banting, F.G., Best, C.H., Collip, J.B., Campbell, W.R., and Fletcher, A.A. (1922). Pancreatic Extracts in the Treatment of Diabetes Mellitus. Can. Med. Assoc. J. *12*, 141–146.
2. Gepts, W. (1965). Pathologic anatomy of the pancreas in juvenile diabetes mellitus. Diabetes *14*, 619–633. https://doi.org/10.2337/diab.14.10.619.
3. Bottazzo, G.F., Florin-Christensen, A., and Doniach, D. (1974). Islet-cell antibodies in diabetes mellitus with autoimmune polyendocrine deficiencies. Lancet *2*, 1279–1283. https://doi.org/10.1016/s0140-6736(74)90140-8.
4. Todd, J.A., Bell, J.I., and McDevitt, H.O. (1987). HLA-DQ beta gene contributes to susceptibility and resistance to insulin-dependent diabetes mellitus. Nature *329*, 599–604.
5. Polychronakos, C., and Li, Q. (2011). Understanding type 1 diabetes through genetics: advances and prospects. Nat. Rev. Genet. *12*, 781–792. https://doi.org/10.1038/nrg3069.
6. Acha-Orbea, H., and McDevitt, H.O. (1987). The first external domain of the nonobese diabetic mouse class II I-A beta chain is unique. Proc. Natl. Acad. Sci. USA *84*, 2435–2439.
7. Postow, M.A., Sidlow, R., and Hellmann, M.D. (2018). Immune-Related Adverse Events Associated with Immune Checkpoint Blockade. N. Engl. J. Med. *378*, 158–168. https://doi.org/10.1056/NEJMra1703481.
8. Wright, J.J., Salem, J.E., Johnson, D.B., Lebrun-Vignes, B., Stamatouli, A., Thomas, J.W., Herold, K.C., Moslehi, J., and Powers, A.C. (2018). Increased Reporting of Immune Checkpoint Inhibitor-Associated Diabetes. Diabetes Care *41*, e150–e151. https://doi.org/10.2337/dc18-1465.
9. Ansari, M.J.I., Salama, A.D., Chitnis, T., Smith, R.N., Yagita, H., Akiba, H., Yamazaki, T., Azuma, M., Iwai, H., Khoury, S.J., et al. (2003). The programmed death-1 (PD-1) pathway regulates autoimmune diabetes in nonobese diabetic (NOD) mice. J. Exp. Med. *198*, 63–69. https://doi.org/10.1084/jem.20022125.
10. Johnson, M.B., Ogishi, M., Domingo-Vila, C., De Franco, E., Wakeling, M.N., Imane, Z., Resnick, B., Williams, E., Galão, R.P., Caswell, R., et al. (2024). Human inherited PD-L1 deficiency is clinically and immunologically less severe than PD-1 deficiency. J. Exp. Med. *221*, e20231704. https://doi.org/10.1084/jem.20231704.
11. Carrero, J.A., McCarthy, D.P., Ferris, S.T., Wan, X., Hu, H., Zinselmeyer, B.H., Vomund, A.N., and Unanue, E.R. (2017). Resident macrophages of pancreatic islets have a seminal role in the initiation of autoimmune diabetes of NOD mice. Proc. Natl. Acad. Sci. USA *114*, E10418–E10427. https://doi.org/10.1073/pnas.1713543114.
12. Calderon, B., Suri, A., Miller, M.J., and Unanue, E.R. (2008). Dendritic cells in islets of Langerhans constitutively present beta cell-derived peptides bound to their class II MHC molecules. Proc. Natl. Acad. Sci. USA *105*, 6121–6126. https://doi.org/10.1073/pnas.0801973105.
13. Calderon, B., Carrero, J.A., Ferris, S.T., Sojka, D.K., Moore, L., Epelman, S., Murphy, K.M., Yokoyama, W.M., Randolph, G.J., and Unanue, E.R. (2015). The pancreas anatomy conditions the origin and properties of resident macrophages. J. Exp. Med. *212*, 1497–1512. https://doi.org/10.1084/jem.20150496.
14. Gautier, E.L., Shay, T., Miller, J., Greter, M., Jakubzick, C., Ivanov, S., Helft, J., Chow, A., Elpek, K.G., Gordonov, S., et al. (2012). Gene-expression profiles and transcriptional regulatory pathways that underlie the identity and diversity of mouse tissue macrophages. Nat. Immunol. *13*, 1118–1128. https://doi.org/10.1038/ni.2419.
15. Costanzo, A., Clarke, D., Holt, M., Sharma, S., Nagy, K., Tan, X., Kain, L., Abe, B., Luce, S., Boitard, C., et al. (2024). Repositioning the Early Pathology of Type 1 Diabetes to the Extraislet Vasculature. J. Immunol. *212*, 1094–1104. https://doi.org/10.4049/jimmunol.2300769.
16. Bottazzo, G.F., Dean, B.M., McNally, J.M., MacKay, E.H., Swift, P.G., and Gamble, D.R. (1985). In situ characterization of autoimmune phenomena and expression of HLA molecules in the pancreas in diabetic insulitis. N. Engl. J. Med. *313*, 353–360.
17. Morgan, N.G. (2024). Insulitis in human type 1 diabetes: lessons from an enigmatic lesion. Eur. J. Endocrinol. *190*, R1–R9. https://doi.org/10.1093/ejendo/lvae002.
18. Coppieters, K.T., Dotta, F., Amirian, N., Campbell, P.D., Kay, T.W.H., Atkinson, M.A., Roep, B.O., and von Herrath, M.G. (2012). Demonstration of islet-autoreactive CD8 T cells in insulitic lesions from recent onset and long-term type 1 diabetes patients. J. Exp. Med. *209*, 51–60. https://doi.org/10.1084/jem.20111187.

19. Li, Y., Zhou, G., Ozaki, T., Nishihara, E., Matsuzuka, F., Bai, Y., Liu, Z., Taniguchi, E., Miyauchi, A., and Kakudo, K. (2012). Distinct histopathological features of Hashimoto's thyroiditis with respect to IgG4-related disease. Mod. Pathol. *25*, 1086–1097. https://doi.org/10.1038/modpathol.2012.68.

20. Palade, G.E., Simionescu, M., and Simionescu, N. (1979). Structural aspects of the permeability of the microvascular endothelium. Acta Physiol. Scand. Suppl. *463*, 11–32.

21. Pober, J.S., and Sessa, W.C. (2014). Inflammation and the blood microvascular system. Cold Spring Harb. Perspect. Biol. *7*, a016345. https://doi.org/10.1101/cshperspect.a016345.

22. Pober, J.S., and Sessa, W.C. (2007). Evolving functions of endothelial cells in inflammation. Nature reviews *7*, 803–815. https://doi.org/10.1038/nri2171.

23. Bonner-Weir, S., and Orci, L. (1982). New perspectives on the microvasculature of the islets of Langerhans in the rat. Diabetes *31*, 883–889. https://doi.org/10.2337/diab.31.10.883.

24. Schwartz, R.H. (2003). T cell anergy. Annu. Rev. Immunol. *21*, 305–334. https://doi.org/10.1146/annurev.immunol.21.120601.141110.

25. Katakai, T., Hara, T., Sugai, M., Gonda, H., and Shimizu, A. (2004). Lymph node fibroblastic reticular cells construct the stromal reticulum via contact with lymphocytes. J. Exp. Med. *200*, 783–795. https://doi.org/10.1084/jem.20040254.

26. Schiavinato, A., Przyklenk, M., Kobbe, B., Paulsson, M., and Wagener, R. (2021). Collagen type VI is the antigen recognized by the ER-TR7 antibody. Eur. J. Immunol. *51*, 2345–2347. https://doi.org/10.1002/eji.202149263.

27. Thiriot, A., Perdomo, C., Cheng, G., Novitzky-Basso, I., McArdle, S., Kishimoto, J.K., Barreiro, O., Mazo, I., Triboulet, R., Ley, K., et al. (2017). Differential DARC/ACKR1 expression distinguishes venular from non-venular endothelial cells in murine tissues. BMC Biol. *15*, 45. https://doi.org/10.1186/s12915-017-0381-7.

28. Picelli, S., Faridani, O.R., Björklund, A.K., Winberg, G., Sagasser, S., and Sandberg, R. (2014). Full-length RNA-seq from single cells using Smart-seq2. Nat. Protoc. *9*, 171–181. https://doi.org/10.1038/nprot.2014.006.

29. Giladi, A., Cohen, M., Medaglia, C., Baran, Y., Li, B., Zada, M., Bost, P., Blecher-Gonen, R., Salame, T.M., Mayer, J.U., et al. (2020). Dissecting cellular crosstalk by sequencing physically interacting cells. Nat. Biotechnol. *38*, 629–637. https://doi.org/10.1038/s41587-020-0442-2.

30. LeBleu, V.S., and Neilson, E.G. (2020). Origin and functional heterogeneity of fibroblasts. Faseb J *34*, 3519–3536. https://doi.org/10.1096/fj.201903188R.

31. Liu, Z., Li, J.P., Chen, M., Wu, M., Shi, Y., Li, W., Teijaro, J.R., and Wu, P. (2020). Detecting Tumor Antigen-Specific T Cells via Interaction-Dependent Fucosyl-Biotinylation. Cell *183*, 1117–1133.e19. https://doi.org/10.1016/j.cell.2020.09.048.

32. Wetzel, S.A., McKeithan, T.W., and Parker, D.C. (2005). Peptide-specific intercellular transfer of MHC class II to CD4+ T cells directly from the immunological synapse upon cellular dissociation. J. Immunol. *174*, 80–89. https://doi.org/10.4049/jimmunol.174.1.80.

33. Scott, N.A., Zhao, Y., Krishnamurthy, B., Mannering, S.I., Kay, T.W.H., and Thomas, H.E. (2018). IFNgamma-Induced MHC Class II Expression on Islet Endothelial Cells Is an Early Marker of Insulitis but Is Not Required for Diabetogenic CD4(+) T Cell Migration. Front. Immunol. *9*, 2800. https://doi.org/10.3389/fimmu.2018.02800.

34. Serreze, D.V., Holl, T.M., Marron, M.P., Graser, R.T., Johnson, E.A., Choisy-Rossi, C., Slattery, R.M., Lieberman, S.M., and DiLorenzo, T.P. (2004). MHC class II molecules play a role in the selection of autoreactive class I-restricted CD8 T cells that are essential contributors to type 1 diabetes development in nonobese diabetic mice. J. Immunol. *172*, 871–879. https://doi.org/10.4049/jimmunol.172.2.871.

35. Gioia, L., Holt, M., Costanzo, A., Sharma, S., Abe, B., Kain, L., Nakayama, M., Wan, X., Su, A., Mathews, C., et al. (2019). Position beta57 of I-A(g7) controls early anti-insulin responses in NOD mice, linking an MHC susceptibility allele to type 1 diabetes onset. Sci. Immunol. *4*, eaaw6329. https://doi.org/10.1126/sciimmunol.aaw6329.

36. Holt, M., Costanzo, A., Gioia, L., Abe, B., Su, A.I., and Teyton, L. (2018). Gene Profiling and T Cell Receptor Sequencing from Antigen-Specific CD4 T Cells. Methods Mol. Biol. *1712*, 217–238. https://doi.org/10.1007/978-1-4939-7514-3_14.

37. Ng, C.T., Nayak, B.P., Schmedt, C., and Oldstone, M.B.A. (2012). Immortalized clones of fibroblastic reticular cells activate virus-specific T cells during virus infection. Proc. Natl. Acad. Sci. USA *109*, 7823–7828. https://doi.org/10.1073/pnas.1205850109.

38. Krenning, G., Zeisberg, E.M., and Kalluri, R. (2010). The origin of fibroblasts and mechanism of cardiac fibrosis. J. Cell. Physiol. *225*, 631–637. https://doi.org/10.1002/jcp.22322.

39. Lumelsky, N., Blondel, O., Laeng, P., Velasco, I., Ravin, R., and McKay, R. (2001). Differentiation of embryonic stem cells to insulin-secreting structures similar to pancreatic islets. Science *292*, 1389–1394. https://doi.org/10.1126/science.1058866.

40. Geusz, R.J., Wang, A., Chiou, J., Lancman, J.J., Wetton, N., Kefalopoulou, S., Wang, J., Qiu, Y., Yan, J., Aylward, A., et al. (2021). Pancreatic progenitor epigenome maps prioritize type 2 diabetes risk genes with roles in development. eLife *10*, e59067. https://doi.org/10.7554/eLife.59067.

41. Pagliuca, F.W., Millman, J.R., Gürtler, M., Segel, M., Van Dervort, A., Ryu, J.H., Peterson, Q.P., Greiner, D., and Melton, D.A. (2014). Generation of functional human pancreatic beta cells in vitro. Cell *159*, 428–439. https://doi.org/10.1016/j.cell.2014.09.040.

42. Bogers, W.M., Stad, R.K., van Es, L.A., and Daha, M.R. (1991). Immunoglobulin A: interaction with complement, phagocytic cells and endothelial cells. Complement Inflamm. *8*, 347–358. https://doi.org/10.1159/000463206.

43. Wan, X., and Unanue, E.R. (2018). Antigen recognition in autoimmune diabetes: a novel pathway underlying disease initiation. Precis. Clin. Med. *1*, 102–110. https://doi.org/10.1093/pcmedi/pby015.

44. Wan, X., Vomund, A.N., Peterson, O.J., Chervonsky, A.V., Lichti, C.F., and Unanue, E.R. (2020). The MHC-II peptidome of pancreatic islets identifies key features of autoimmune peptides. Nat. Immunol. *21*, 455–463. https://doi.org/10.1038/s41590-020-0623-7.

45. Wan, X., Zinselmeyer, B.H., Zakharov, P.N., Vomund, A.N., Taniguchi, R., Santambrogio, L., Anderson, M.S., Lichti, C.F., and Unanue, E.R. (2018). Pancreatic islets communicate with lymphoid tissues via exocytosis of insulin peptides. Nature *560*, 107–111. https://doi.org/10.1038/s41586-018-0341-6.

46. Perez-Shibayama, C., Gil-Cruz, C., and Ludewig, B. (2019). Fibroblastic reticular cells at the nexus of innate and adaptive immune responses. Immunol. Rev. *289*, 31–41. https://doi.org/10.1111/imr.12748.

47. Siegert, S., and Luther, S.A. (2012). Positive and negative regulation of T cell responses by fibroblastic reticular cells within paracortical regions of lymph nodes. Front. Immunol. *3*, 285. https://doi.org/10.3389/fimmu.2012.00285.

48. Sharma, S., Tan, X., Boyer, J., Clarke, D., Costanzo, A., Abe, B., Kain, L., Holt, M., Armstrong, A., Rihanek, M., et al. (2023). Measuring anti-islet autoimmunity in mouse and human by profiling peripheral blood antigen-specific CD4 T cells. Sci. Transl. Med. *15*, eade3614. https://doi.org/10.1126/scitranslmed.ade3614.

49. Wang, J., Yoshida, T., Nakaki, F., Hiai, H., Okazaki, T., and Honjo, T. (2005). Establishment of NOD-Pdcd1-/- mice as an efficient animal model of type I diabetes. Proc. Natl. Acad. Sci. USA *102*, 11823–11828. https://doi.org/10.1073/pnas.0505497102.

50. Bretscher, P.A. (1999). A two-step, two-signal model for the primary activation of precursor helper T cells. Proc. Natl. Acad. Sci. USA *96*, 185–190. https://doi.org/10.1073/pnas.96.1.185.

51. Sckisel, G.D., Bouchlaka, M.N., Monjazeb, A.M., Crittenden, M., Curti, B.D., Wilkins, D.E.C., Alderson, K.A., Sungur, C.M., Ames, E., Mirsoian, A., et al. (2015). Out-of-Sequence Signal 3 Paralyzes Primary CD4(+)

T-Cell-Dependent Immunity. Immunity *43*, 240–250. https://doi.org/10.1016/j.immuni.2015.06.023.

52. Ragazzo, J.L., Ozaki, M.E., Karlsson, L., Peterson, P.A., and Webb, S.R. (2001). Costimulation via lymphocyte function-associated antigen 1 in the absence of CD28 ligation promotes anergy of naive CD4+ T cells. Proc. Natl. Acad. Sci. USA *98*, 241–246. https://doi.org/10.1073/pnas.98.1.241.
53. Frauwirth, K.A., Alegre, M.L., and Thompson, C.B. (2000). Induction of T cell anergy in the absence of CTLA-4/B7 interaction. J. Immunol. *164*, 2987–2993. https://doi.org/10.4049/jimmunol.164.6.2987.
54. Quill, H., and Schwartz, R.H. (1987). Stimulation of normal inducer T cell clones with antigen presented by purified Ia molecules in planar lipid membranes: specific induction of a long-lived state of proliferative nonresponsiveness. J. Immunol. *138*, 3704–3712.
55. Jenkins, M.K., Chen, C.A., Jung, G., Mueller, D.L., and Schwartz, R.H. (1990). Inhibition of antigen-specific proliferation of type 1 murine T cell clones after stimulation with immobilized anti-CD3 monoclonal antibody. J. Immunol. *144*, 16–22.
56. Buckley, C.D., Pilling, D., Lord, J.M., Akbar, A.N., Scheel-Toellner, D., and Salmon, M. (2001). Fibroblasts regulate the switch from acute resolving to chronic persistent inflammation. Trends Immunol. *22*, 199–204. https://doi.org/10.1016/s1471-4906(01)01863-4.
57. Yoshida, K., Corper, A.L., Herro, R., Jabri, B., Wilson, I.A., and Teyton, L. (2010). The diabetogenic mouse MHC class II molecule I-Ag7 is endowed with a switch that modulates TCR affinity. J. Clin. Investig. *120*, 1578–1590. https://doi.org/10.1172/JCI41502.
58. Rizk, A.A., Dybala, M.P., Rodriguez, K.C., Slak Rupnik, M., and Hara, M. (2023). Pancreatic regional blood flow links the endocrine and exocrine diseases. J. Clin. Investig. *133*, e166185. https://doi.org/10.1172/JCI166185.
59. Slak Rupnik, M., and Hara, M. (2024). Local Dialogues Between the Endocrine and Exocrine Cells in the Pancreas. Diabetes *73*, 533–541. https://doi.org/10.2337/db23-0760.
60. Bingley, P.J., Bonifacio, E., Williams, A.J., Genovese, S., Bottazzo, G.F., and Gale, E.A. (1997). Prediction of IDDM in the general population: strategies based on combinations of autoantibody markers. Diabetes *46*, 1701–1710. https://doi.org/10.2337/diab.46.11.1701.
61. Bonifacio, E., and Achenbach, P. (2019). Birth and coming of age of islet autoantibodies. Clin. Exp. Immunol. *198*, 294–305. https://doi.org/10.1111/cei.13360.
62. Sorini, C., Cosorich, I., Lo Conte, M., De Giorgi, L., Facciotti, F., Lucianò, R., Rocchi, M., Ferrarese, R., Sanvito, F., Canducci, F., and Falcone, M. (2019). Loss of gut barrier integrity triggers activation of islet-reactive T cells and autoimmune diabetes. Proc. Natl. Acad. Sci. USA *116*, 15140–15149. https://doi.org/10.1073/pnas.1814558116.
63. Mobasseri, M., Shirmohammadi, M., Amiri, T., Vahed, N., Hosseini Fard, H., and Ghojazadeh, M. (2020). Prevalence and incidence of type 1 diabetes in the world: a systematic review and meta-analysis. Health Promot. Perspect. *10*, 98–115. https://doi.org/10.34172/hpp.2020.18.
64. Iannuzzi, J.P., King, J.A., Leong, J.H., Quan, J., Windsor, J.W., Tanyingoh, D., Coward, S., Forbes, N., Heitman, S.J., Shaheen, A.A., et al. (2022). Global Incidence of Acute Pancreatitis Is Increasing Over Time: A Systematic Review and Meta-Analysis. Gastroenterology *162*, 122–134. https://doi.org/10.1053/j.gastro.2021.09.043.
65. Klein, A.P. (2019). Pancreatic cancer: a growing burden. Lancet Gastroenterol. Hepatol. *4*, 895–896. https://doi.org/10.1016/S2468-1253(19)30323-1.
66. Vilarrasa, N., San Jose, P., Rubio, M.Á., and Lecube, A. (2021). Obesity in Patients with Type 1 Diabetes: Links, Risks and Management Challenges. Diabetes Metab. Syndr. Obes. *14*, 2807–2827. https://doi.org/10.2147/DMSO.S223618.
67. Calder, P.C. (2010). Omega-3 fatty acids and inflammatory processes. Nutrients *2*, 355–374. https://doi.org/10.3390/nu2030355.
68. Williams, T., Krovi, H.S., Landry, L.G., Crawford, F., Jin, N., Hohenstein, A., DeNicola, M.E., Michels, A.W., Davidson, H.W., Kent, S.C., et al. (2018). Development of T cell lines sensitive to antigen stimulation. J. Immunol. Methods *462*, 65–73. https://doi.org/10.1016/j.jim.2018.08.011.
69. Holst, J., Vignali, K.M., Burton, A.R., and Vignali, D.A.A. (2006). Rapid analysis of T-cell selection in vivo using T cell-receptor retrogenic mice. Nat. Methods *3*, 191–197. https://doi.org/10.1038/nmeth858.
70. Khan, M., and Gasser, S. (2016). Generating Primary Fibroblast Cultures from Mouse Ear and Tail Tissues. J. Vis. Exp. *10*, 53565. https://doi.org/10.3791/53565.

STAR★METHODS

KEY RESOURCES TABLE

REAGENT or RESOURCE	SOURCE	IDENTIFIER
Antibodies		
Anti-TCRβ-APC (H57-597)	BioLegend	BioLegend Cat# 109212, RRID:AB_313435
Anti-CD3 (2C11)	In-house	N/A
Anti-CD28 (37.51)	BioXcell	Bio X Cell Cat# BE0015-1, RRID: AB_1107624
Anti-CD45-Biotin (30-F11)	BioLegend	BioLegend Cat# 103103, RRID:AB_312968
Anti-Biotin-PE (1D4-C5)	BioLegend	BioLegend Cat# 409004, RRID: AB_10641847
Anti-CD4-APC-Cy7 (RM4-5)	BioLegend	BioLegend Cat# 100526, RRID:AB_312727
Anti-Vβ8.1/8.2-FITC (MR5-2)	BD Pharmingen	BD Biosciences Cat# 553185, RRID: AB_394694
Anti-Vβ4-FITC (KT4)	BD Biosciences	BD Biosciences Cat# 553365, RRID: AB_394811
Anti-CD19-Bv510 (6D5)	BioLegend	BioLegend Cat# 115545, RRID: AB_2562136
Anti-CD45-FITC (30-F11)	BD Pharmingen	BD Biosciences Cat# 553079, RRID: AB_394609
Anti-MHC-class II-PE (OX-6)	BioLegend	BioLegend Cat# 107608, RRID:AB_313323
Anti-CD31-PE-Cy7 (MEC13.3)	BioLegend	BioLegend Cat# 102523, RRID: AB_2572181
Anti-gp38-APC-Cy7 (8.1.1)	BioLegend	BioLegend Cat# 127417, RRID: AB_2629803
Anti-CD11b-APC (M1/70)	BioLegend	BioLegend Cat# 101212, RRID:AB_312795
Anti-HLA-DR-Bv421 (L243)	BioLegend	BioLegend Cat# 307636, RRID: AB_2561831
Anti-CD276 antibody (EPNCIR122)	Abcam	Abcam Cat# ab134161, RRID:AB_2687929
Ant-CD276 antibody (MJ8)	Sigma-Aldrich	Millipore Cat# 04–1501, RRID: AB_10615633
anti-B7H4 polyclonal	Thermo Fisher Scientific	Bioss Cat# bs-0673R, RRID:AB_10857690
Anti-PD-L1 antibody (EPR19759)	Abcam	Abcam Cat# ab213524, RRID:AB_2857903
anit CD31 antibody (P2B1)	Abcam	Abcam Cat# ab24590, RRID:AB_448167
Anti-CD31 (MEC 7.46)	Abcam	Abcam Cat# ab7388, RRID:AB_305905
Anti-Insulin polyclonal	Agilent	Agilent Cat# A0564, RRID:AB_10013624
Fibroblast Antibody (ER-TR7)	BioRad	Bio-Rad Cat# MCA2402, RRID:AB_915429
Anti-DARC Polyclonal Antibody	Invitrogen	Scientific Cat# PA5-112940, RRID: AB_2867674
Anti-DARC Polyclonal Antibody	Invitrogen	Scientific Cat# PA5-47861, RRID: AB_2576815
AG2.42.7	In-house	N/A
Anti-HLA-DR antibody (HLA-Pan/2967R)	Abcam	Novus Cat# NBP2-79709, RRID: AB_3404931
Anti-CD45-FITC (HI30)	BioLegend	BioLegend Cat# 304006, RRID:AB_314394
Biological samples		
NOD/LtJ mice	Jackson Laboratory	RRID:IMSR_001976
NOD.Cg-Tg(TcrαBDC2.5,TcrβBDC2.5)	Jackson Laboratory	RRID:IMSR_004460
NOD/LtJ H2A−/−	Jackson Laboratory	RRID:IMSR_003583
NOD.Cg-Tg(TCRα8F10,TCRβ8F10)	Dr. E. Unanue, Washington University	N/A

(*Continued on next page*)

Continued

REAGENT or RESOURCE	SOURCE	IDENTIFIER
Human islets Patient A	IIDP, Prodo Laboratories	RRID: SAMN181976260
Human islets Patient B	IIDP, Prodo Laboratories	RRID: SAMN18528866
Human islets Patient C	IIDP, Prodo Laboratories	RRID: SAMN20082921
Human islets Patient D	IIDP, Prodo Laboratories	RRID: SMN20209569
Human islets Patient E	IIDP, Prodo Laboratories	RRID: SAMN20478103
Non-diabetic and diabetic human pancreatic tissue	nPOD, MyBiosource	RRID: SCR_014641
Chemicals, peptides, and recombinant proteins		
Dulbecco's modified Eagle's medium (DMEM)	Corning	Cat# 10-013-CV
Fetal bovine serum (FBS)	Thermo Fisher Scientific	Cat# SH3008803HI
L-glutamine	Corning	Cat# 25-005-CI
Penicillin/Streptomycin	Corning	Cat# 30-002-CI
Collagenase P	Sigma-Aldrich	Cat# 11213857001
Trypsin EDTA	Corning	Cat# 25-052-CI
Histopaque-1077	Sigma-Aldrich	Cat# 10771
GDP-fucose-biotin	Peng Wu Scripps Reserach	N/A
GDP-fucose	Peng Wu Scripps Reserach	N/A
pHrodo Deep Red E. coli BioParticles	Invitrogen	Cat# P35366
Normal Goat Serum (NGS)	Abcam	Cat# ab7481
Fish Gelatin	Fisher Scientific	Cat# Fisher Scientific
Slowfade Gold antifade reagent with DAPI	Life Technologies	Cat# S36938
Critical commercial assays		
Miltenyi $CD4^+$ isolation kit	Miltenyi	Cat# 130-104-454
Deposited data		
Single cell RNA-seq and single cell rT-qPCR data	This paper	Geo number
Experimental models: Cell lines		
5KC (TCR$\alpha-\beta-$) cells	Dr. Nakayama, University of Colorado	N/A
Phoenix-ECO retro viral packaging cells	ATCC	CRL 3214 RRID:SCR_003163
H1 human Embryonic Stem Cells (hESCs)	Maike Sander UCSD	N/A
Experimental models: Organisms/strains		
NOD/LtJ mice	Jackson Laboratory	RRID:IMSR_001976
NOD.Cg-Tg(TcrαBDC2.5,TcrβBDC2.5)	Jackson Laboratory	RRID:IMSR_004460
NOD/LtJ H2A$-/-$	Jackson Laboratory	RRID:IMSR_003583
NOD.Cg-Tg(TCRα8F10,TCRβ8F10)	Dr. E. Unanue, Washington University	N/A
Oligonucleotides		
Primers for gene expression analysis	Table S1	N/A
Recombinant DNA		
pLenti CMV/TO SV40 small + Large T (w612-1)	Addgene	RRID:Addgene_22298
psPAX2	Addgene	RRID:Addgene_12260
VSV.G	Addgene	RRID:Addgene_14888
pMSCV-IRES-GFP II (pMIG II)	Addgene	RRID:Addgene_52107
pMIG-hFUT6	Peng Wu Scripps Reserach	N/A
Software and algorithms		
Fluidigm Real-time PCR Analysis software	Fluidigm	RRID:SCR_015686
Seurat	Version 5.0.1	RRID:SCR_007322
Nextflow	Version 24.10.5	RRID:SCR_024135

(*Continued on next page*)

Continued

REAGENT or RESOURCE	SOURCE	IDENTIFIER
Data accessible at Gene Expression Omnibus website (accession number GSE292898).		N/A
Other		
Astrios Moflo cell sorter	Beckman Coulter	RRID:SCR_018893
Biomark HD unit	Fluidigm	BMKHD-BMKHD
96 × 96 Dynamic Array flowcells	Fluidigm	BMK-*M*-96.96
NextSeq2000 sequencer	Illumina	RRID:SCR_023614
Zeiss 780 confocal microscope	Zeiss	RRID:SCR_020922
EVOS M5000 inverted microscope	Invitrogen	RRID:SCR_023650
MACSquant analyzer 10	Miltenyi	RRID:SCR_020268
mTeSR1 media	Stem Cell Technologies	Cat #85850
Matrigel	Corning	Cat #354230
Versene Solution	Gibco	Cat #15040
Y-27632	Stem Cell Technologies	Cat #72307
Accutase	Thermo Fisher Scientific	A1110501

EXPERIMENTAL MODEL AND STUDY PARTICIPANT DETAILS

Mice

NOD/LtJ mice were purchased from the Jackson laboratory. NOD.Cg-Tg(TcraBDC2.5,TcrbBDC2.5) and NOD/LtJ mice with a deletion of MHC class II genes, referred in the text as NOD H2A$^{-/-}$, were also from the Jackson laboratory [NODCaj.129S2(B6)-H2-Ab1tm1Doi/LwnJ]. NOD.Cg-Tg (TCRa8F10, TCRb8F10) were a generous gift of Dr. E. Unanue (Washington University, St Louis). All animals were genotyped before being used in experiments. Care and handling of mice under pathogen-free conditions at our animal facility followed Institutional Animal Care and Use Committee rules.

Cell lines

5KC (TCR$\alpha-\beta-$) cells, a generous gift from Dr. Nakayama (University of Colorado)[68] were maintained in Dulbecco's modified Eagle's medium (DMEM10)–10% fetal bovine serum (HyClone FBS) with L-glutamine, penicillin, and streptomycin (Corning). For re-expression of TCRs in 5KC cells, after sequencing Vα and Vβ segments were synthesized and cloned into pMIG-II[69] using Hifi Gibson Assembly (New England Biolabs) and spinfected with polybrene for 1 h at 32°C, at 2000g. After recovery, cells expressing TCR were sorted by flow cytometry after staining with anti–TCRβ-APC antibody (H57-597, BioLegend).

Phoenix-ECO packaging cells Phoenix-ECO cells were cultured in DMEM10 and used for retro viral packaging of the PMIG-II based vectors.

H1 hESCs H1 human embryonic stem cells were maintained as described[40]; briefly, cells were seeded on 1:100 Matrigel (Corning 356238) in mTeSR1 medium (Stemcell Technologies 85850).

None of the cell lines were tested for Mycoplasma but all were used only in short-term culture.

Human tissues

Non-diabetic and diabetic pancreatic tissue was obtained through nPOD and MyBiosource (MBS640801).

Fresh human islets from five non-diabetic donors (ages/BMI: 41–28, 32–25.7, 62–20.6, 45–21.9, 30–25.4) were supplied by IIDP for study "Lymphatics of the islet and T cell trafficking." (IIDP, Prodo laboratories).

METHOD DETAILS

Re-expression of TCRs in 5KC cells

After sequencing, Vα and Vβ segments were synthesized and cloned into pMIG-II[69] using NEB HiFi Gibson Assembly. 5KC cells were spinfected (2000 g, 32°C, 1 h) with viral supernatant plus polybrene (8ug/ml). TCR-expressing cells were recovered overnight and sorted using anti-TCRβ-APC (H57-597, BioLegend).

T cell hybridoma stimulation assay

Increasing numbers of islets were co-cultured with 4 × 10^4 T cell hybridomas per flat-bottom 96-well plate. After 24 h at 37°C, supernatants were assayed for IL-2 using an IL-2-dependent bioassay.

Primary T cell stimulation assays

Spleen $CD4^+$ T cells were isolated after mincing the tissue and sieving it through a 70 μm nylon screen using a rubber syringe plunger. After erythrocytes removal by osmotic lysis, $CD4^+$ cells were purified using negative selection (Miltenyi $CD4^+$ isolation kit). Purity as assessed by CD4/Vβ staining and flow cytometry was >95%. On average 10×10^6 8F10 or BDC2.5 splenocytes yielded 2×10^6 pure cells.

Single-cell flow cytometry sorting for T cell assays

Cells were stained in 30 μL FACS buffer, PBS with 2% FBS and 2 mM EDTA, with Vβ8.1/8.2-FITC (8F10) or Vβ4-FITC (BDC2.5), CD4-APC-Cy7, and propidium iodide (1 μg mL^{-1}). Single live cells were sorted (Astrios MoFlo) into 96-well PCR plates containing 5 μL RT mix. Pre-amp and Biomark HD qPCR were performed as described.[35,36]

Fucosylation-biotinylation (FucoID) assay

A TFRC1-93–FUT640-359 fusion was expressed via pMIG-II in activated splenocytes. GFP+ cells (2–5 × 104) were co-cultured with 150 dissociated islets (DMEM10 + 20 mM $MgCl_2$, 37°C, 2–3 h). GDP-fucose-biotin (80 μM, 20 min, RT) was quenched with GDP-fucose (300 μM, 10 min). Cells were washed and stained with anti-biotin-PE antibody and PI; PI^-/$Biotin^+$ single cells were sorted for RT-qPCR.

Human islet single-cell flow cytometry and sorting

Dissociated human islets were prepared by trypsin-EDTA digestion (20 min, ice) and stained with HLA-DR-BV421 and CD45-FITC. PI^-/$CD45^-$/$HLA\text{-}DR^+$ or PI^-/$CD45^+$/$HLA\text{-}DR^+$ cells were sorted into 96-well PCR plates.

Mouse islet isolation and single-cell flow cytometry

Pancreata were perfused with collagenase P (0.5 mg mL^{-1}) and digested (37°C, 17 min). Slurry was filtered (0.419 mm mesh). A density gradient was established by layering Histopaque 1077 and serum-free RPMI; sample was loaded on top. After centrifugation (600 g, 20 min), islets were collected at the interface, washed, and hand-picked. Yield: 300–400 islets per mouse. For single-cell suspension, islets were digested with trypsin-EDTA and washed. Cells were stained with MHC II-PE and CD45-FITC antibodies; PI^-/$CD45^-$/$MHC\ II^+$ or PI^-/$CD45^+$/$MHC\ II^+$ cells were sorted into 96-well PCR plates.

SMART-seq2 library preparation

Sequencing libraries were prepared from microtiter plates containing 1 cell per well sorted in reverse transcription buffer. The entire volume from each well, 5 ∫L, was used with the Takara SMARTer HT library prep kit following manufacturers recommended protocol. Briefly, first strand cDNA synthesis was performed with template switching followed by 19 cycles of PCR. PCR products were quantitated using the Thermo Fisher Qubit system. For each sample 150 pgs of cDNA was then used for tagmentation followed by an additional 12 cycles of PCR with 96 unique indexed PCR primers. Samples were then pooled in groups of 48 and purified using Ampure XP beads (0.6×). Library pools were then quantitated (Qubit) and Bioanalyzed (Agilent Bioanalyzer 2100) before loading onto a NextSeq2000 sequencer (Illumina) to generate 101 base single reads with 8 base i5 and 8 base i7 index reads. Samples were sequenced using one P2 flowcell for each batch on 96 samples.

Primary skin fibroblast isolation

Tails and ears from NOD mice were processed as described with slight alterations[70]. Briefly, tails and ears were dissected and soaked in 90% ethanol for 5 min. To digest the tissue, minced pieces were re-suspended in DMEM 10% FBS with 2.5mg/ml collagenase P (Roche) for 90 min while shaking at 37°C. The digested products were pushed through a 70mm nylon screen with the rubber plunger of a 3mL syringe. The digestion was stopped with PBS containing 2mM EDTA. Cells were resuspended in DMEM 10% FBS at a density of 2 mice per 10cm dish. Cells were cultured for 6 days.

Immunofluorescence of frozen pancreatic sections

Pancreas were excised and embedded in O.C.T Compound. Tissue sectioned at 7.0 ∫m and fixed using 4%PFA for 15 min. After washing several times with PBS, tissue permeabilized using 0.2% Triton X-100, 15min, and blocked in 5% NGS/5% Fish Gelatin for 30min. Primary antibodies diluted in blocking buffer and incubated from 2 hr-o/n at 4°C. Sections washed and incubated in secondary antibody at room temperature for 40min-1hr. DAPI was used for nuclear counterstain. All co-staining were carried out sequentially. Images were acquired using a Zeiss 780 confocal microscope.

Phagocytosis assays

For flow cytometry, 1×10^5 SV40 transformed islet fibroblasts were plated with or without 100 ∫g/mL of pHrodo Deep Red E. coli BioParticles in 96 well plates. After 1 h incubation at 37°C, cells were washed with PBS, trypsinized, and resuspended in FACS buffer. Cell suspensions were analyzed using a MACSquant analyzer 10 (Miltenyi).

For imaging, 1×10^5 SV40 transformed islet fibroblasts were plated onto glass coverslips in 80 ∫L droplets with or without pHrodo Deep Red E. coli BioParticle (Invitrogen). Cells were washed with PBS prior to fixation with 4% PFA for 3 min. Cells were washed three times with PBS following fixation. A small amount of water was used to remove residual PBS. Coverslips were placed onto slides with one drop of Slowfade Gold antifade reagent with DAPI (Life Technologies), then the edges were cemented with clear nail polish. Bright field, DAPI, and Cy5 images were captured with a EVOS M5000 inverted microscope (Invitrogen) at 40× magnification.

Maintenance and differentiation of H1 hESCs (procedure)

H1 hESCs were maintained as described.[40] In brief, hESCs were seeded onto 1:100 Matrigel (Corning, 356238) coated tissue culture surfaces in mTeSR1 media (Stem Cell Technologies, 85850) and propagated every 3 to 4 days. Versene Solution (Gibco, 15040-066) dissociation method was employed for passaging and 10 ∫M Y-27632 (Stem Cell Technologies, 72307) was supplied on the first day of each passage. Accutase (Thermo Fisher Scientific, 00-4555-56) base enzymatic dissociation method and 10 ∫M Y-27632 were employed to generate a single-cell suspension, enabling precise cell counting to plate the appropriate cell concentration to initiate the differentiation.

At day 0), undifferentiated cells were washed in Stage 1/2 base medium and then differentiated using a seven-step protocol with stage-specific medium.[40]

QUANTIFICATION AND STATISTICAL ANALYSIS

For single cell RT-qPCR experiments (see Table S1), the front analysis was performed using the Fluidigm suite of software. Ct values below 30 were included if melting curves were within 1°C of expected values for each primer set. Statistical analysis and data visualization were done in R using Seurat69. Cells with no signal and genes with no signal were removed prior to analysis. Ct values were transformed using the function (30-Ct)∧2 and log normalized in Seurat. *p* values were calculated using Wilcoxon Rank-Sum.

For single cell SMARTseq experiments, upstream data processing steps were performed using the nf-core RNA-seq version 3.3 pipeline. Built using Nextflow, the pipeline processes data using the following steps: preprocessing, alignment and quantification, alignment post-processing, transcript assembly and quantification, coverage visualization, quality control, pseudo-alignment and quantification.[70] Cells with less than 1000 counts and genes with no signal were removed. Only cells with MHC class II transcript were included in analysis. *p* values were calculated using a Wilcox rank-sum test. Statistical significance was established if *p* values were <0.05 after adjusting for multiple comparisons using a Bonferroni correction. For the violin plots in Figure 3, *p* values were calculated using a two-tailed students t-test.

For expression correlation studies, average counts per million were used to perform Kendall tau-b calculations (Figure 7).